

**The functions of SARS-CoV-2 neutralizing and infection-enhancing antibodies
in vitro and in mice and nonhuman primates**

Dapeng Li^{1,2*}, Robert J Edwards^{1,2*}, Kartik Manne^{1,2*}, David R. Martinez^{3,*}, Alexandra Schäfer^{3,*}, S. Munir Alam^{1,2}, Kevin Wiehe^{1,2}, Xiaozhi Lu^{1,2}, Robert Parks^{1,2}, Laura L. Sutherland^{1,2}, Thomas H. Oguin III^{1,2}, Charlene McDanal⁴, Lautaro G. Perez⁴, Katayoun Mansouri^{1,2}, Sophie M. C. Gobeil^{1,2}, Katarzyna Janowska^{1,2}, Victoria Stalls^{1,2}, Megan Kopp^{1,2}, Fangping Cai^{1,2}, Esther Lee^{1,2}, Andrew Foulger^{1,2}, Giovanna E. Hernandez^{1,2}, Aja Sanzone^{1,2}, Kadamawit Tilahun^{1,2}, Chuancang Jiang^{1,2}, Longping V. Tse³, Kevin W. Bock⁴, Mahnaz Minai⁴, Bianca M. Nagata⁴, Kenneth Cronin^{1,2}, Victoria Gee-Lai^{1,2}, Margaret Deyton^{1,2}, Maggie Barr^{1,2}, Tarra Von Holle^{1,2}, Andrew N. Macintyre^{1,2}, Erica Stover^{1,2}, Jared Feldman⁶, Blake M. Hauser⁶, Timothy M. Caradonna⁶, Trevor D. Scobey³, M. Anthony Moody^{1,7}, Derek W. Cain^{1,2}, C. Todd DeMarco^{1,2}, Thomas N. Denny^{1,2}, Christopher W. Woods^{1,2,8}, Elizabeth W. Petzold⁸, Aaron G. Schmidt^{6,9}, I-Ting Teng¹⁰, Tongqing Zhou¹⁰, Peter D. Kwong^{10,11}, John R. Mascola¹⁰, Barney S. Graham¹⁰, Ian N. Moore⁴, Robert Seder¹⁰, Hanne Andersen¹², Mark G. Lewis¹², David C. Montefiori⁵, Gregory D. Sempowski^{1,2}, Ralph S. Baric³, Priyamvada Acharya^{1,5}, Barton F. Haynes^{1,2,13,#}, Kevin O. Saunders^{1,5,13,14,#}

¹Duke Human Vaccine Institute, Duke University School of Medicine, Durham, NC 27710, USA

²Department of Medicine, Duke University School of Medicine, Durham, NC 27710, USA

³Department of Epidemiology, University of North Carolina at Chapel Hill, Chapel Hill, NC 27599, USA

⁴Infectious Disease Pathogenesis Section, Comparative Medicine Branch, National Institute of Allergy and Infectious Diseases, National Institutes of Health, Bethesda, MD 20892, USA.

⁵Department of Surgery, Duke University, Durham, NC 27710, USA

⁶Ragon Institute of MGH, MIT and Harvard, Cambridge, MA 02139, USA

⁷Department of Pediatrics, Duke University School of Medicine, Durham, NC 27710, USA

⁸Center for Applied Genomics and Precision Medicine, Duke University Medical Center, Durham, NC 27710, USA

⁹Department of Microbiology, Harvard Medical School, Boston, MA 02115, USA

28 ¹⁰Vaccine Research Center, National Institute of Allergy and Infectious Diseases (NIAID), NIH, Bethesda, MD
29 20892, USA

30 ¹¹Department of Biochemistry and Molecular Biophysics, Columbia University, New York, NY 10032, USA

31 ¹²BIOQUAL, Rockville, MD 20850, USA

32 ¹³Department of Immunology, Duke University School of Medicine, Durham, NC 27710, USA

33 ¹⁴Department of Molecular Genetics and Microbiology, Duke University School of Medicine, Durham, NC 27710,
34 USA

35

36 *Co-First Authors

37 #Correspondence: barton.haynes@duke.edu (B.F.H.) and kevin.saunders@duke.edu (K.O.S.)

38

39 **Summary (135 words)**

40 SARS-CoV-2 neutralizing antibodies (NAbs) protect against COVID-19, making them a focus of vaccine
41 design. A safety concern regarding SARS-CoV-2 antibodies is whether they mediate disease enhancement. Here,
42 we isolated potent NAbs against the receptor-binding domain (RBD) and the N-terminal domain (NTD) of SARS-
43 CoV-2 spike protein from individuals with acute or convalescent SARS-CoV-2 or a history of SARS-CoV-1
44 infection. Cryo-electron microscopy of RBD and NTD antibodies demonstrated function-specific modes of
45 antibody binding. Select RBD NAbs also demonstrated Fc receptor- γ (Fc γ R)-mediated enhancement of virus
46 infection *in vitro*, while five non-neutralizing NTD antibodies mediated Fc γ R-independent *in vitro* infection
47 enhancement. However, both *in vitro* neutralizing and infection-enhancing RBD or infection-enhancing NTD
48 antibodies protected from SARS-CoV-2 challenge in non-human primates and mice. One of 30 monkeys infused
49 with enhancing antibodies had lung pathology and bronchoalveolar lavage cytokine evidence suggestive of
50 enhanced disease. Thus, these *in vitro* assessments of enhanced antibody-mediated infection do not necessarily
51 indicate biologically relevant *in vivo* infection enhancement.

52
53 **Keywords**

54 SARS-CoV-2, COVID-19, neutralizing antibody, receptor-binding domain, N-terminal domain, electron
55 micrograph, *in vivo* protection, infection enhancement

56

57 **Introduction**

58 The severe acute respiratory syndrome coronavirus 2 (SARS-CoV-2) has caused a global pandemic with over
59 43 million cases and 1.16 million deaths (<https://coronavirus.jhu.edu/>). Development of combinations of
60 neutralizing antibodies for prevention or treatment of infection can significantly help to control the pandemic,
61 while the ultimate solution to control the COVID-19 pandemic is a safe and effective vaccine (Graham, 2020;
62 Sempowski et al., 2020).

63 Neutralizing antibodies (NAbs) that can block viral entry are crucial for controlling virus infections (Battles
64 and McLellan, 2019; Corti and Lanzavecchia, 2013; Dashti et al., 2019). Previously reported SARS-CoV and
65 MERS-CoV NAbs function by targeting the receptor-binding domain (RBD) or the N-terminal domain (NTD) of
66 spike (S) protein to block receptor binding, or by binding to the S2 region of S protein to interfere with S2-
67 mediated membrane fusion (Du and Jiang, 2010; Jiang et al., 2020; Xu et al., 2019). Importantly, prophylactic or
68 therapeutic use of SARS-CoV-2 NAbs in non-human primates (Shi et al., 2020) or rodent models (Hassan et al.,
69 2020; Rogers et al., 2020; Wu et al., 2020b) showed protection from SARS-CoV-2-induced lung inflammation
70 and/or reduction in viral load. SARS-CoV-2 NAbs reported to date predominantly target the RBD region (Baum et
71 al., 2020; Brouwer et al., 2020a; Cao et al., 2020; Chen et al., 2020; Hansen et al., 2020; Ju et al., 2020; Liu et al.,
72 2020a; Pinto et al., 2020; Robbiani et al., 2020; Rogers et al., 2020; Shi et al., 2020; Wang et al., 2020a; Wrapp et
73 al., 2020a; Wu et al., 2020b). In contrast, NTD antibodies that neutralize SARS-CoV-2 are rare and of modest
74 neutralization potency (Brouwer et al., 2020b; Chi et al., 2020; Wec et al., 2020; Zost et al., 2020a; Zost et al.,
75 2020b).

76 Antibody-dependent enhancement (ADE) of infection *in vitro* has been reported with a number of viruses.
77 ADE has been associated with vaccination for respiratory syncytial virus (RSV), with vaccination for dengue virus,
78 or with dengue virus infection (Arvin et al., 2020). ADE is often mediated by Fc receptors for IgG (FcγRs),
79 complement receptors (CRs) or both, and is most commonly observed in cells of monocyte/macrophage and B cell
80 lineages (Iwasaki and Yang, 2020; Ubol and Halstead, 2010). *In vitro* studies have demonstrated FcγR-mediated
81 ADE of SARS-CoV-1 infection of ACE2-negative cells (Jaume et al., 2011; Kam et al., 2007; Wan et al., 2020;
82 Wang et al., 2014; Yilla et al., 2005; Yip et al., 2016; Yip et al., 2014). One group demonstrated FcγR-independent
83 infection enhancement of SARS-CoV-1 in Vero cells, and isolated a monoclonal antibody that was suggested to
84 induce enhanced lung viral load and pathology *in vivo* (Wang et al., 2016). The ability of antibodies that bind the

85 SARS-CoV-2 S protein to mediate infection enhancement *in vivo* is unknown but is a theoretical concern for
86 COVID-19 vaccine development (Arvin et al., 2020; Bournazos et al., 2020; Iwasaki and Yang, 2020).

87 Here, we identified potent *in vitro* neutralizing RBD and NTD antibodies as well as *in vitro* infection-
88 enhancing RBD and NTD antibodies from individuals infected with SARS-CoV-1 or SARS-CoV-2. Negative stain
89 electron microscopy (NSEM) and cryo-electron microscopy (cryo-EM) revealed distinct binding patterns and the
90 precise epitopes of infection-enhancing and neutralizing antibodies. *In vitro* studies using human FcγR-expressing
91 or ACE2-expressing cell lines demonstrated that the RBD antibodies mediated FcγR-dependent infection
92 enhancement, whereas the NTD antibodies induced FcγR-independent infection enhancement. However, using
93 monkey and mouse models of SARS-CoV-2 infection, none of these infection-enhancing antibodies consistently
94 augmented SARS-CoV-2 lung viral load, infectious virus in the lung, or lung disease pathology *in vivo*. Rather, one
95 of 30 monkeys had lung pathology and bronchoalveolar lavage (BAL) cytokine levels suggestive of enhanced lung
96 disease. *In vitro* infection-enhancing antibodies prevented or reduced virus replication in cynomolgus macaques or
97 mice challenged with SARS-CoV-2, SARS-CoV-2 mouse-adapted (MA) viruses (Dinnon et al., 2020b; Leist et al.,
98 2020a), or bat WIV1-coronavirus (CoV) (Menachery et al., 2016). Thus, the *in vitro* infection enhancing activity of
99 SARS-CoV-2 RBD and NTD antibodies only rarely translated to *in vivo* relevance.

100

101 **RESULTS**

102 **Isolation of infection-enhancing SARS-CoV-2 antibodies**

103 SARS-CoV-2-reactive human monoclonal antibodies from plasmablasts or SARS-CoV-2-reactive memory B
104 cells were isolated by flow cytometric sorting (Liao et al., 2009; Liao et al., 2013) from a SARS-CoV-2 infected
105 individual 11, 15, 36, and 70 days post-onset of symptoms. Additional memory B cells were isolated from an
106 individual infected with SARS-CoV-1 ~17 years prior to sample collection (**Figures 1A-B, S1 and S2**). We
107 isolated and characterized 1,737 antibodies, which bound to SARS-CoV-2 S and nucleocapsid (NP) proteins
108 (**Figure 1C; Table S1**). We selected 187 antibodies for further characterization, and first examined neutralization
109 of SARS-CoV-2 pseudovirus and replication-competent SARS-CoV-2. Forty-four of 81 recombinant RBD
110 antibodies exhibited neutralization when assayed in 293T/ACE-2 cell pseudovirus, SARS-CoV-2
111 microneutralization, or SARS-CoV-2 plaque reduction assays (**Figures S3A-F; Tables S2-S3**).

112 Ten of the forty-one NTD antibodies neutralized in the 293T/ACE2 pseudovirus and plaque reduction assays,
113 with the most potent antibody neutralizing pseudovirus with an IC₅₀ of 39 ng/mL (**Figures S3G-I; Tables S4-S5**).
114 In addition, 5 non-neutralizing NTD antibodies enhanced SARS-CoV-2 pseudovirus infection in 293T/ACE2 cells
115 by 56% to 148% (**Figure 1D**). To determine whether this effect was applicable to replication-competent virus, we
116 tested these five antibodies for enhancement of SARS-CoV-2 virus infection of Vero cells. Infection of replication-
117 competent SARS-CoV-2 nano-luciferase virus (Hou et al., 2020) also increased in the presence of each of the 5
118 NTD antibodies (**Figure 1E**). Analysis of *in vitro* enhancement of NTD antibodies in ACE2-negative TZM-bl cells
119 demonstrated no infection enhancement, suggesting enhancement-dependence on ACE2. Both ACE2-expressing
120 293T cells used for pseudovirus assays and Vero cells lack FcγR expression (Takada et al., 2007). Thus, NTD
121 enhancement of SARS-CoV-2 infection was FcγR-independent.

122 Previous studies have demonstrated FcγR-mediated ADE of SARS-CoV-1 infection in ACE2-negative cells
123 (Jaume et al., 2011; Kam et al., 2007; Wan et al., 2020; Wang et al., 2014; Yilla et al., 2005; Yip et al., 2016; Yip
124 et al., 2014). Here, FcγR-dependent infection enhancement was determined by generating stable TZM-bl cell lines
125 that expressed individual human FcγRs (FcγRI, FcγRIIa, FcγRIIb or FcγRIII). TZM-bl cells naturally lack ACE-2
126 and TMPRSS2 receptors, thus SARS-CoV-2 was unable to infect FcγR-negative TZM-bl cells (**Figure 1F**). One
127 hundred S-reactive IgG1 antibodies selected from **Tables S2-S7** were tested for their ability to facilitate SARS-
128 CoV-2 infection of TZM-bl cells. Three of the antibodies enabled SARS-CoV-2 infection of TZM-bl cells
129 expressing FcγRI, and five antibodies mediated infection of FcγRIIb-expressing TZM-bl cells (**Figures 1F-J**). The
130 antigen-binding fragments (Fabs) of these antibodies did not mediate infection enhancement of TZM-bl cells
131 expressing FcγRI or FcγRIIb (**Figures 1K-L**). FcγRI and FcγRIIb-dependent infection-enhancing antibodies were
132 specific for the RBD of S protein, consistent with a recent finding by another group using COVID-19 patient sera
133 or a recombinant antibody (Wu et al., 2020a). Thus, RBD antibodies can be either neutralizing in the 293T/ACE2
134 cell line, infection-enhancing in the TZM-bl-FcγR-expressing cell lines, or both (**Figure 2A**). NTD antibodies can
135 either be neutralizing or infection-enhancing in the 293T/ACE2 cell line or Vero E6 cells (**Figure 2A**). Therefore,
136 the repertoire of SARS-CoV-2 antibodies included potent neutralizing RBD and NTD antibodies, FcγR-dependent,
137 infection-enhancing RBD antibodies, and FcγR-independent infection-enhancing NTD antibodies.

139 **Characterization of infection-enhancing Spike recombinant antibodies**

140 We compared the phenotypes and binding modes to S protein for five infection-enhancing RBD antibodies
141 and three RBD antibodies that lacked infection enhancement to elucidate differences between these two types of
142 antibodies. All selected RBD antibodies neutralized SARS-CoV-2 pseudovirus and/or replication-competent virus
143 in ACE2-expressing cells (**Figures 2A and S5**), despite five of these antibodies mediating infection enhancement
144 in ACE2-negative, Fc γ R-positive TZM-bl cells (**Figures 1F-L, 2A, and S5**). Both types of selected RBD antibodies
145 blocked ACE2 binding to S protein. Fabs of four of the infection-enhancing RBD antibodies and two of the non-
146 infection-enhancing RBD antibodies bound to S with high affinities ranging from 0.1 to 9 nM (**Figures S6-8**).
147 Thus, the infection-enhancing or non-enhancing RBD antibodies showed similarities in ACE2 blocking, affinity,
148 and neutralization of ACE2-dependent SARS-CoV-2 infection (**Figure 2A**).

149 We obtained NSEM reconstructions of Fabs in complex with stabilized S ectodomain trimer for six
150 representative RBD antibodies (Hsieh et al., 2020). Infection-enhancing RBD antibodies DH1041 and DH1043
151 bound with a vertical approach (**Figure 2B**), parallel to the central axis of the S trimer, similar to non-infection-
152 enhancing antibodies DH1042 and DH1044 (**Figure 2C**). The epitopes of antibodies DH1041, DH1042, and
153 DH1043 overlapped with that of the ACE-2 receptor (Wang et al., 2020b), consistent with their ability to block
154 ACE-2 binding to S protein (**Figure 2A and S10**). Their epitopes were similar to those of three recently described
155 antibodies, P2B-2F6 (Ju et al., 2020), H11-H4, and H11-D4 (**Figure S10**) (Huo et al., 2020; Zhou et al., 2020). The
156 epitope of another non-infection-enhancing RBD antibody DH1044 was only slightly shifted relative to DH1041,
157 DH1042 and DH1043 (**Figure 2C**), but resulted in DH1044 not blocking ACE2 binding (**Figure 2A and S10**). The
158 remaining two RBD antibodies, DH1045 and DH1047 cross-reacted with both SARS-CoV-1 and SARS-CoV-2 S
159 (**Figure 2A and S4**). Although DH1047 mediated Fc γ R-dependent infection of TZM-bl cells and DH1045 did not,
160 both antibodies bound to RBD-up S conformations with a more horizontal angle of approach (**Figure 2B-C and**
161 **S10**) (Pak et al., 2009). Thus, epitopes and binding angles of RBD antibodies determined by NSEM did not
162 discriminate between antibodies that mediated Fc γ R-dependent infection enhancement and those that did not.

163 We performed similar comparative analyses of five Fc γ R-independent, infection-enhancing NTD antibodies,
164 and five non-infection-enhancing NTD antibodies (DH1048, DH1049, DH1051, DH1050.1 and DH1050.2) that
165 neutralized SARS-CoV-2 (pseudovirus IC₅₀ titers 39 - 520 ng/mL; SARS-CoV-2 plaque reduction IC₅₀ titers 390 -

166 780 ng/mL) (**Figure 2A and S5C-D**). The Fabs of neutralizing antibodies DH1050.1 and DH1051 bound to
167 stabilized S ectodomain with affinities of 16 and 19 nM respectively, whereas the infection-enhancing antibody
168 DH1052 bound with 294 nM affinity (**Figures S6-8**). NSEM reconstructions obtained for nine of the ten NTD
169 antibodies showed that the Fc γ R-independent, infection-enhancing NTD antibodies (DH1053-DH1056) bound to S
170 with their Fab constant domains directed downward toward the virus membrane (**Figure 2D**), whereas the five
171 neutralizing NTD-directed Abs (DH1048-DH1051) bound to S with the constant domain of the Fab directed
172 upward away from the virus membrane (**Figure 2E**). Thus, S protein antibody epitopes and binding modes were
173 associated with Fc γ R-independent, infection-enhancing activity of NTD antibodies. The five neutralizing
174 antibodies bound the same epitope as antibody 4A8 (Wrapp et al., 2020a), with three of the five having the same
175 angle of approach as 4A8 (**Figure S11**). Interestingly, the NTD antibodies with the same angle of approach as 4A8,
176 were also genetically similar to 4A8, being derived from the same V_H1-24 gene segment (**Table S8**), although their
177 light chains were different (Wrapp et al., 2020a). These antibodies may constitute a neutralizing antibody class that
178 can be reproducibly elicited upon SARS-CoV-2 infection.

179

180 **Competition between infection-enhancing and non-infection enhancing antibodies**

181 To determine whether infection-enhancing antibodies could compete with non-infection-enhancing antibodies
182 for binding to S ectodomain, we performed surface plasmon resonance (SPR) competitive binding assays. RBD
183 antibodies segregated into two clusters, where antibodies within a cluster blocked each other and antibodies in
184 different clusters did not block each other (**Figures 3A and S12**). One cluster included antibodies DH1041,
185 DH1043 and DH1044, and the other cluster included antibodies DH1046 and DH1047. NSEM reconstructions
186 showed DH1041 and DH1047 Fabs bound simultaneously to different epitopes of the stabilized S trimer (**Figure**
187 **3B**). Similarly, DH1043 and DH1047 Fabs also bound simultaneously to different epitopes on the stabilized S
188 protein (**Figure 3B**).

189 NTD antibodies also segregated into two clusters based on their ability to block each other (**Figure 3A**).

190 Neutralizing NTD antibodies blocked each other and formed one cluster, while infection-enhancing/non-

191 neutralizing NTD antibodies blocked each other and formed a second cluster (**Figures 3A, 3C, S12 and S13**).

192 NSEM reconstruction of SARS-CoV-2 S trimer bound with Fabs of neutralizing NTD antibody DH1050.1 and

193 infection-enhancing NTD antibody DH1052 confirmed that the two antibodies could simultaneously bind to
194 distinct epitopes on a single SARS-CoV-2 S trimer (**Figure 3D**). DH1054 was unique as it was able to block both
195 infection-enhancing and neutralizing NTD antibodies (**Figures 3C and S13**).

196 NTD antibodies did not compete with RBD antibodies for binding to S trimer (**Figure 3A**). This result gave
197 rise to the notion that in a polyclonal mixture of antibodies, the SARS-CoV-2 S trimer could bind both RBD and
198 NTD antibodies. To determine the potential for this complex to form, we liganded SARS-CoV-2 S trimer with Fabs
199 of each type of antibody and visualized the complex using NSEM. NSEM showed that neutralizing RBD antibodies
200 could also bind to the same S protomer as neutralizing NTD antibodies DH1050.1 or DH1051 (**Figure 3E**).
201 Moreover, we found that a single S protomer could be simultaneously occupied by two RBD antibodies (DH1043
202 and DH1047) and an NTD antibody (DH1050.1) (**Figure 3F**). Thus, the S trimer could simultaneously bind to
203 multiple RBD and NTD neutralizing antibody Fabs.

204

205 **FcγR-independent infection-enhancement in the presence of neutralizing antibodies**

206 The NSEM determination of antibody binding modes demonstrated that certain infection-enhancing antibodies
207 and non-infection enhancing antibodies bound to distinct epitopes on the same S protomer (**Figures 3A-F**). Thus,
208 we determined the functional outcome of infection-enhancing antibodies binding to S in the presence of
209 neutralizing antibodies. We examined whether a FcγR-independent, infection-enhancing NTD antibody could
210 inhibit RBD antibody neutralization of ACE-2-mediated SARS-CoV-2 pseudovirus infection of 293T/ACE2 cells
211 *in vitro*. We hypothesized that the outcome would be dependent on which antibody was present at the highest
212 concentration. We examined RBD antibody DH1041 neutralization in the presence of 132 and 1,325-fold excess of
213 infection-enhancing NTD antibody DH1052. DH1041 neutralization activity was minimally decreased in the
214 presence of 132-fold excess of DH1052. When DH1041 neutralization was assessed in the presence of 1,325-fold
215 excess of antibody DH1052, infection enhancement was observed when DH1041 concentration was below 10
216 ng/mL (**Figures 3G and S14**). A nearly identical result was obtained when we examined neutralization by DH1043
217 (**Figures 3H and S14**). Thus, a ~1000-fold excess of infection-enhancing NTD antibody was required to out-
218 compete the effect of a potent RBD neutralizing antibody *in vitro*.

219

220 **Cryo-EM structural determination of RBD and NTD-directed antibody epitopes**

221 To visualize atomic level details of their interactions with the S protein, we selected representatives from the
222 panels of RBD and NTD-directed antibodies for structural determination by cryo-EM. Of the RBD-directed
223 antibodies, we selected two (DH1041 and DH1043) that most potently neutralized SARS-CoV-2 virus in the
224 293T/ACE2 pseudovirus assay and also enhanced infection in TZM-bl-FcγRI or -FcγRIIb cells. We also selected
225 the RBD-directed antibody DH1047, which shared the infection enhancing and ACE-2 blocking properties of
226 DH1041 and DH1043, but unlike DH1041 and DH1043, DH1047 also showed reactivity with the SARS-CoV-1 S
227 protein. From the panel of NTD-directed antibodies, we selected one infection-enhancing NTD antibody, DH1052,
228 and one neutralizing NTD antibody, DH1050.1, for higher resolution structural determination by cryo-EM. The
229 stabilized SARS-CoV-2 S ectodomain “2P” (S-2P) (Wrapp et al., 2020b) was used for preparing complexes for
230 structural determination.

231 For all three RBD-directed antibodies, the cryo-EM datasets revealed heterogeneous populations of S protein
232 with at least one RBD in the “up” position (**Figures 4, S15 and S16**). We did not find any unliganded S or any 3-
233 RBD-down S population, even though the unliganded S-2P consistently shows a 1:1 ratio of 1-RBD-up and 3-
234 RBD-down populations (Henderson et al., 2020; Walls et al., 2020), suggesting that binding of the RBD-directed
235 antibodies to S protein alters RBD dynamics. All S-2P trimers were stoichiometrically bound to 3 Fabs, with
236 antibodies bound to both up and down RBDs in an S-2P trimer.

237 We observed that the primary epitopes of DH1041 and DH1043 were centered on the Receptor Binding Motif
238 (RBM; residues 483-506) of the RBD (**Figures 4A-B, S17 and S18**), providing structural basis for the ACE-2
239 blocking phenotype of these antibodies. While DH1041 utilized its heavy chain complementarity determining
240 regions (CDRs) to contact the RBM, the DH1043 paratope included both its heavy and light chains.

241 Unlike the RBM-focused epitope of DH1041 and DH1043, the epitope of antibody DH1047 was focused
242 around the $\alpha 2$ and $\alpha 3$ helices and $\beta 2$ strand that are located outside the N-terminus of the RBM (**Figures 4C and**
243 **S19**)(Ju et al., 2020). Contact is also made by RBD residues 500-506 that are also outside the RBM but at its C-
244 terminal end, and stack against the N-terminal end of the $\alpha 3$ helix providing a continuous interactive surface for
245 DH1047 binding. The DH1047 paratope included heavy chain complementarity determining regions HCDR2,
246 HCDR3 and light chain LCDR1 and LCDR3. The HCDR3 stacks against and interacts with the residues in the $\beta 2$
247 strand. Interactions with the $\beta 2$ strand are also mediated by HCDR2. Similar to DH1041 and DH1043, the DH1047

248 interacted with an “up” RBD conformation from an adjacent protomer although these interactions were not well-
249 characterized due to disorder in that region.

250 We next determined cryo-EM structures of the NTD-directed neutralizing antibodies, DH1050.1 (**Figure 4D**)
251 and NTD-directed infection-enhancing antibody, DH1052 (**Figure 4E**), at 3.4 Å and 3.0 Å resolutions,
252 respectively. Unlike the RBD-directed antibodies DH1041, DH1043 and DH1047, where we only observed spikes
253 with at least one RBD in the up position, the cryo-EM datasets of DH1050.1- and DH1052-bound complexes
254 showed antibody bound to both 3-RBD-down and 1-RBD-up S-2P spikes (**Figures S20-S21**). Consistent with the
255 NSEM reconstructions, the neutralizing antibody DH1050.1 and the non-neutralizing, infection-enhancing antibody
256 DH1052 bound opposite faces of the NTD, with the epitope for the neutralizing antibody DH1050.1 facing the host
257 cell membrane and the epitope for the non-neutralizing, infection-enhancing antibody DH1052 facing the viral
258 membrane. The dominant contribution to the DH1050.1 epitope came from NTD loop region 140-158 that stacks
259 against the antibody HCDR3 and extends farther into a cleft formed at the interface of the DH1050.1 HCDR1,
260 HCDR2 and HCDR3 loops. The previously described NTD antibody 4A8 interacts with the same epitope in a
261 similar elongated HCDR3-dominated manner making similar contacts, although DH1050.1 and 4A8 (Chi et al.,
262 2020) show a rotation about the stacked HCDR3 and NTD 140-158 loops, suggesting focused recognition of the
263 elongated NTD loop by a class of antibodies sharing the same VH origin. Consistent with their diverse light chain
264 gene origins, the light chains of DH1050.1 and 4A8 do not contact the S protein. The focused recognition of the
265 NTD loop 140-158 by DH1050.1 is reminiscent of the interactions that HIV-1 fusion peptide-directed antibodies
266 make with the HIV-1 Env, where recognition is focused on the conserved region of the flexible fusion peptide
267 (Dingens et al., 2018; Xu et al., 2018). In a structurally conserved mechanism, such focused recognition is
268 characterized by robust cryo-EM density at the recognition site but increased disorder away from the site of
269 focused interactions (**Figures 4E and S21**).

270 The infection enhancing NTD-directed antibody DH1052 bound the NTD at an epitope facing the viral
271 membrane and comprised of residues spanning 27-32, 59-62 and 211-218, with all the CDR loops of both heavy
272 and light chains involved in contacts with the NTD. We also observed contact of the antibody with the glycan at
273 position 603, as well as the conformationally invariant SD2 region.

274 Thus, we found that the RBD-directed antibodies isolated in this study influenced RBD dynamics and bound
275 only to spike with at least one RBD in the up conformations, and in some cases, also induced the 2-RBD-up and 3-

276 RBD-up spike conformations. In contrast, the NTD-directed antibodies bound to both the 3-RBD-down and 1-
277 RBD-up spikes that are present in the unliganded S-2P. Our results provide a structural explanation for the ACE-2
278 blocking activity of RBD-directed antibodies as well as for the cross-reactivity of the DH1047 antibody. We
279 observed two distinct orientations for the NTD-directed antibodies that are either neutralizing or non-neutralizing,
280 with the former binding the NTD surface that faces away from the viral membrane and the latter binding the
281 surface that faces the viral membrane.

282

283 **NTD antibodies that mediate SARS-CoV-2 infection enhancement *in vitro*, do not necessarily enhance** 284 **infection or disease in murine and macaque models of infection**

285 To determine the biological relevance of *in vitro* infection enhancement by NTD antibodies, we assessed
286 enhanced SARS-CoV-2 acquisition or disease severity *in vivo* in a COVID-19 disease mouse model of aged
287 BALB/c mice challenged with the mouse-adapted SARS-CoV-2 MA10 strain (Leist et al., 2020a). The FcγR-
288 independent, *in vitro* infection-enhancing antibody DH1052 or a control influenza antibody CH65 were given 12
289 hours prior to SARS-CoV-2 MA10 infection (**Figure 5A**). Throughout the four days of infection, DH1052-infused
290 mice exhibited similar levels of body weight loss and higher survival than mice given negative control IgG (2/9
291 control mice died while 0/10 DH1052-treated mice died) (**Figures 5B-C**). In addition, DH1052-treated mice
292 exhibited lower lung hemorrhagic scores, lower lung viral titers and lower lung tissue subgenomic RNA levels
293 compared to control IgG-infused mice (**Figures 5D-F**). Overall, DH1052 treatment resulted in less severe disease
294 and reduced viral replication rather than infection enhancement. Therefore, NTD antibodies that enhanced infection
295 *in vitro* did not enhance infection or disease *in vivo* in the SARS-CoV-2 MA10 virus infection mouse model.

296 Next, we examined the effect of infusion of NTD antibody DH1052 on SARS-CoV-2 infection in monkeys
297 (Leist et al., 2020b; Rockx et al., 2020). Cynomolgus macaques were infused with 10 mg of antibody per kilogram
298 of body weight and then challenged intranasally and intratracheally with 10⁵ plaque forming units of SARS-CoV-2
299 three days later (**Figure 5G**) (54). We compared the protective activity of *in vitro* infection-enhancing antibody
300 DH1052, neutralizing NTD antibody DH1050.1, and negative control influenza antibody CH65 in separate groups
301 of macaques. While no human antibody was detected pre-infusion (**Figure 5H**), antibody infusion resulted in
302 human antibody concentrations ranging from 11 to 238 μg/mL in serum at day 2 post-challenge (**Figure 5I and**
303 **S26A-D**). Sera with DH1050.1 neutralized SARS-CoV-2 pseudovirus at a mean ID₅₀ titer of 19 (**Figure 5J**), and

304 neutralized SARS-CoV-2 replication-competent virus at a mean ID₅₀ titer of 192 (**Figure 5K**). In contrast, the
305 presence of DH1052 or control antibody CH65 in serum did not neutralize SARS-CoV-2 (**Figure 5J-K**).
306 Macaques that received CH65 or DH1052 had comparable lung inflammation four days after infection (**Figures**
307 **5L, S22 and S23A**). However, one macaque administered DH1052 showed increased perivascular mononuclear
308 inflammation, perivascular and alveolar edema (**Figure S23B**), and multiple upregulated bronchoalveolar fluid
309 (BAL) cytokines (**Figure S24-S25**) compared to either control antibody-infused animals or the four other monkeys
310 in the DH1052-treated group. In contrast, macaques administered DH1050.1, a neutralizing NTD antibody, had
311 lower lung inflammation than CH65-infused macaques (**Figures 5L, S22 and S23A**). Infusion of either neutralizing
312 NTD DH1050.1 or *in vitro* infection-enhancing antibody DH1052 reduced viral nucleocapsid antigen in the lung
313 (**Figures 5M, S22 and S23A**). Envelope (E) gene subgenomic RNA (sgRNA) and nucleocapsid (N) gene sgRNA
314 in the BAL were also reduced in macaques that were administered DH1050.1 or DH1052 compared to macaques
315 treated with negative control antibody (**Figures 5N-O and S26G**). In nasal swab fluid, macaques showed reduced E
316 and N gene sgRNA when DH1050.1 or DH1052 was infused respectively, with the reduction by DH1050.1 being
317 statistically significant (**Figures 5P-Q, S26E-F and S26H-I**). Thus, neutralizing NTD antibody DH1050.1
318 provided protection against SARS-CoV-2 infection in cynomolgus macaques, while the *in vitro* infection-
319 enhancing antibody DH1052 showed no infection enhancement overall, but rather showed partial protection from
320 SARS-CoV-2 infection.

321

322 **FcγR-dependent, *in vitro* infection-enhancing RBD antibodies do not enhance SARS-CoV-2 infection in mice**

323 We next tested RBD neutralizing antibodies that also mediated infection enhancement in TZM-bl cells
324 expressing FcγRI or FcγRII in a SARS-CoV-2 acquisition mouse model (**Figures 6A-B**). Aged (12 months old)
325 BALB/c mice were injected intraperitoneally with 300 μg of antibody, and challenged with a SARS-CoV-2 mouse-
326 adapted (MA) isolate twelve hours later (Dinnon et al., 2020a). Mice received either FcγR-dependent, *in vitro*
327 infection-enhancing antibody DH1041, non-infection enhancing antibody DH1050.1, or a combination of both
328 antibodies. Administration of RBD NAb DH1041 alone or in combination with DH1050.1 protected all mice from
329 detectable infectious virus in the lungs 48h after challenge (**Figure 6A**). In the setting of therapeutic treatment,
330 administration of DH1041 alone (300 μg) or in combination with DH1050.1 (150 μg of each) twelve hours after

331 SARS-CoV-2 challenge significantly reduced lung infectious virus titers, with half of the mice having undetectable
332 infectious virus in the lung 48h after challenge (**Figure 6B**). Thus, while RBD antibody DH1041 could mediate
333 Fc γ R-dependent, *in vitro* infection enhancement, it protected mice from SARS-CoV-2 infection when administered
334 prophylactically or therapeutically.

335 DH1046 and DH1047 are RBD antibodies that neutralize SARS-CoV, SARS-CoV-2 and bat WIV1-CoV
336 (Menachery et al., 2016) (**Figure 2A, S4A-B, S5E-H and S27**). Both of these RBD antibodies mediated Fc γ R-
337 dependent, *in vitro* SARS-CoV-2 infection enhancement of TZM-bl cells that lacked ACE-2 expression (**Figures**
338 **1F-L**). To determine whether SARS-CoV-2 *in vitro* infection enhancement predicted *in vivo* infection enhancement
339 by SARS-related bat coronaviruses, we assessed the ability of either DH1046 or DH1047 to enhance or protect
340 against bat WIV1-CoV infection in HFH4-ACE2-transgenic mice. Mice were challenged either 12 hours before or
341 12 hours after intraperitoneal injection of antibody (**Figures 6C-D**). Mice administered DH1046 or DH1047 before
342 challenge had no detectable infectious virus in the lung, whereas control IgG administered mice had a mean titer of
343 84,896 plaque forming units per lung lobe (**Figure 6C**). Administration of DH1047 after challenge eliminated
344 detectable infectious virus in the lung in 3 of 5 mice (**Figure 6D**). Therapeutic administration of DH1046 reduced
345 infectious virus titers 10-fold compared to negative control IgG (**Figure 6D**). Thus, Fc γ R-dependent *in vitro*
346 infection-enhancing RBD antibodies DH1046 and DH1047 did not enhance infection *in vivo*, but rather protected
347 mice from SARS-related bat coronavirus infection.

349 ***In vitro* infection-enhancing RBD antibodies do not enhance SARS-CoV-2 infection in nonhuman primates**

350 Finally, we assessed the *in vivo* relevance of RBD antibody infection enhancement in the cynomolgus
351 macaque SARS-CoV-2 intranasal/intratracheal challenge model. We examined *in vivo* infection enhancement by
352 RBD antibodies DH1041, DH1043, DH1046, and DH1047 that neutralized SARS-CoV-2 pseudovirus and
353 replication-competent virus, but enhanced infection *in vitro* in Fc γ RI or Fc γ RIIb-expressing TZM-bl cells (**Figures**
354 **1 and 6E**). After antibody infusion at 10 mg of antibody per kg of macaque body weight, serum human IgG
355 concentrations reached 11-228 μ g/mL at day 2 post-challenge (**Figure 6F-G and S26A-D**). The same macaque
356 serum containing the RBD antibodies exhibited a wide range of neutralization potency (ID₅₀ titers) against SARS-
357 CoV-2 pseudovirus or replication-competent virus, commensurate with the neutralization potency of each antibody

358 (**Figure 6H and 6I**). Infusion of RBD antibody DH1041, DH1043, or DH1047 resulted *in vivo* protection from
359 SARS-CoV-2 infection. In macaques administered DH1041, DH1043, or DH1047, lung inflammation was reduced
360 and lung viral antigen was undetectable in all but one macaque (**Figures 6J-K, S22 and S23A**). E gene sgRNA and
361 N gene sgRNA were significantly reduced in the upper and lower respiratory tract based on analyses of
362 bronchoalveolar lavage fluid, nasal swabs, and nasal wash samples (**Figures 6L-O and S26E-I**). The RBD
363 antibody DH1046 only protected a subset of infused monkeys. Four monkeys treated with RBD antibody DH1046
364 exhibited the same or lower levels of lung inflammation compared to monkeys that received control IgG (**Figure**
365 **6J**). One DH1046-infused monkey had an increased lung inflammation score compared to control antibody
366 monkeys (**Figures 6J, S22, and S23**), but had not evidence of perivascular or alveolar edema or evidence of
367 abnormal BAL cytokines (**Figures S24-S25**). Comparing the DH1046 group to the control IgG group, viral antigen
368 in the lung was reduced overall (**Figures 6K, S22 and S23A**), however reductions in E gene and N gene sgRNA
369 levels were not significant in BAL or nasal fluid at most timepoints (**Figures 6L-O and S26E-I**). These results
370 further demonstrated that both FcγR-independent and FcγR-dependent *in vitro* SARS-CoV-2 infection
371 enhancement did not translate to SARS-CoV-2 *in vivo* infection enhancement.

372

373 **DISCUSSION**

374 Antibody enhancement of virus infection *in vitro* has been reported for MERS-CoV and SARS-CoV (Gu et al.,
375 2005; Liu et al., 2020a; Wan et al., 2020; Wang et al., 2016) and is a critical question facing the safe administration
376 of antibody prophylaxis, antibody therapy, and antibody-based COVID-19 vaccines (Halstead and Katzelnick,
377 2020; Karthik et al., 2020; Lee et al., 2020; Ulrich et al., 2020). The effects of SARS-CoV-2 antibodies have been
378 further questioned since individuals who seroconverted earlier tend to have more severe COVID-19 disease than
379 later seroconverters (Ho et al., 2005). Here, we demonstrated that SARS-CoV-2 antibodies can mediate infection
380 enhancement *in vitro*. However, this *in vitro* phenotype does not translate to enhanced SARS-CoV-2 or SARS-
381 related virus infection in mice, nor does it usually translate to enhanced infection in a non-human primate model of
382 SARS-CoV-2 infection. We assessed *in vivo* infection enhancement as severe lung immunopathology or increased
383 respiratory tract virus replication. Neither of these hallmarks of infection enhancement was significantly present in
384 mice. Two of 30 monkeys administered RBD or NTD antibodies that mediate infection enhancement *in vitro* had
385 increased lung inflammation despite having low or undetectable lung viral antigen. One of these two macaques had

386 lung histology and BAL cytokine levels suggestive of antibody-mediated enhanced pathology. However, these
387 indicators of antibody-mediated enhancement were not present in all macaques that received the same antibody,
388 thus host-specific differences may have influenced the pathology outcomes. These preclinical results indicate that
389 SARS-CoV-2 antibody treatments or the induction of SARS-CoV-2 antibodies by vaccination have a low
390 likelihood of exacerbating COVID-19 disease in humans.

391 It is of interest that a potent therapeutic Spike antibody, LY-CoV555 recently failed to demonstrate efficacy in
392 the treatment of hospitalized patients with COVID-19 (ACTIV-3/TICO LY-CoV555 Study Group,(2020). We
393 observed here that high levels (1,345-fold excess) of enhancing antibodies can overcome effects of neutralizing
394 antibodies and enhance SARS-CoV-2 infection *in vitro* (**Figure S14**). It will be of interest to determine if the lack
395 of efficacy was due to neutralizing effects of LY-CoV555 being outcompeted by infection-enhancing effects of
396 host antibodies.

397 Previous studies with polyclonal serum antibodies against SARS-CoV have also shown *in vitro* Fc γ R-
398 dependent infection enhancement, but no *in vivo* infection enhancement in hamsters (Kam et al., 2007). For the
399 present study, there are two potential explanations for why there is a lack of congruence between *in vitro* infection
400 enhancement assays and outcomes of passive antibody infusion/SARS-CoV-2 challenge studies. First,
401 macrophages and other phagocytes are the target cells that uptake MERS-CoV when infection enhancement occurs
402 (Hui et al., 2020; Wan et al., 2020; Zhou et al., 2014). In contrast, SARS-CoV and SARS-CoV-2 do not
403 productively infect macrophages (Bournazos et al., 2020; Hui et al., 2020; Yip et al., 2016). Thus, while RBD
404 antibodies may be able to mediate Fc γ R-dependent virus uptake of SARS-CoV-2 *in vitro*, *in vivo* Fc γ R-dependent
405 virus uptake of SARS-CoV-2 may largely lead to abortive infection in macrophages (Cheung et al., 2005; Yip et
406 al., 2016).

407 A second potential explanation for a lack of agreement between *in vitro* infection enhancement assays and *in*
408 *vivo* studies is that *in vivo* SARS-CoV-2 antibodies may have the ability to combat SARS-CoV-2 replication
409 through antibody effector functions. While circulating *in vivo*, antibodies can opsonize infected cells or virions and
410 recruit effector immune cells to kill the virus or the infected cells through Fc-mediated mechanisms. A recent study
411 in a SARS-CoV-2 mouse model of acquisition suggested that Fc effector functions contribute to the protective
412 activity of SARS-CoV-2 neutralizing antibodies C104, C002, and C110 (Schafer et al., 2021). Thus, antibody
413 effector functions may contribute to the outcome *in vivo*, but not be accounted for in SARS-CoV-2 neutralization

414 assays *in vitro*. In support of this hypothesis, infection-enhancing, non-neutralizing NTD antibody DH1052
415 reduced infectious virus titers in the lungs of challenged mice compared to the negative control antibody.
416 Consistent with previous findings for human IgG (Dekkers et al., 2017), we have demonstrated that DH1052
417 antibody can bind to murine Fc γ Rs (Alam SM, Li D, Saunders KO, Haynes BF, unpublished), raising the
418 hypothesis that Fc-mediated effector functions may be responsible for the reduction in infectious virus observed in
419 our mouse challenge study. Future studies will investigate the Fc-mediated effector functions of DH1052 to discern
420 their role in reducing infectious SARS-CoV-2 virus titer *in vitro* and *in vivo*.

421 Notably, we observed two different types of *in vitro* infection enhancement. First, RBD antibodies mediated
422 classical antibody-dependent enhancement that required Fc γ Rs for virus uptake (Lee et al., 2020). Previous studies
423 have demonstrated that uptake of MERS-CoV or SARS-CoV has mostly been mediated by Fc γ RIIa on the surface
424 of macrophages (Bournazos et al., 2020; Wan et al., 2020; Yip et al., 2016). In contrast to SARS-CoV and MERS-
425 CoV infection enhancing antibodies, we identified SARS-CoV-2 RBD antibodies utilized Fc γ RIIb or Fc γ RI. Thus,
426 different Fc γ Rs can mediate SARS-CoV and MERS-CoV *in vitro* infection enhancement compared to SARS-CoV-
427 2 *in vitro* infection enhancement. Second, non-neutralizing NTD antibodies mediated Fc γ R-independent infection
428 enhancement in two different Fc γ R-negative, ACE-2-expressing cell types. The mechanism of this *in vitro*
429 enhancement remains unclear, but one hypothesis is the possibility of antibody modulation of S protein
430 conformation. In NSEM studies, NTD antibodies preferentially bound to S in a 3-RBD-down conformation. One
431 study has reported that binding of select NTD antibodies to S enhances S binding to ACE2 (Liu et al., 2020b).
432 Whether S protein has different entry kinetics or higher affinity for ACE-2 when liganded to infection-enhancing
433 antibody DH1052 will be a focus of future studies.

434 There are currently over 100 COVID-19 vaccine candidates under development (Anderson et al., 2020;
435 Corbett et al., 2020a; Corbett et al., 2020b; Folegatti et al., 2020; Jackson et al., 2020; Mulligan et al., 2020; Wrapp
436 et al., 2020b). Both the Pfizer/BioNTech and Moderna mRNA-lipid nanoparticle (LNP) vaccine efficacy trials have
437 completed and showed ~95% vaccine efficacy (Jackson et al., 2020; Polack et al., 2020). The Moderna vaccine
438 trial had 30 severe COVID-19 cases—all in the placebo group—indicating no disease enhancement was seen
439 (www.fda.gov, 2020). It is also important to note that administration of COVID-19 convalescent sera to over
440 35,000 COVID-19 patients have demonstrated the treatment to be safe and is not associated with enhanced disease
441 (Joyner et al., 2020). However, a recent study demonstrated that suboptimal neutralizing antibody level is a

442 significant predictor of severity for SARS-CoV-2 (Garcia-Beltran et al., 2020). Thus it will be important to
443 continue to monitor on-going COVID-19 vaccine efficacy trials for the possibility of vaccine associated enhanced
444 disease (VAED) (Haynes et al., 2020).

445 Our results here indicate while SARS-CoV-2 enhancement occurred in SARS-CoV-2 infection assays *in vitro*,
446 these assays did not always predict infection enhancement in mice or monkeys *in vivo*. Additionally, the SARS-
447 CoV-2-infected individual from whom many of our antibodies were isolated did not progress to severe COVID-19
448 disease. Thus, these results suggest that antibody-induced enhancement of infection is a rare possibility but will not
449 likely be a biologically relevant adverse effect following COVID-19 vaccination in humans.

451 METHODS

452 Detailed methods are provided in the supplemental online material.

454 ACKNOWLEDGMENTS

455 We thank the COVID-19 donors enrolled in the Molecular and Epidemiological Study of Suspected Infection
456 protocol (MESSI), the MESSI clinical support team, the DHVI Clinical Accessioning Unit Core and the DHVI
457 Immunology and Virology Quality Assessment Core for sample procurement, processing and biobanking. We
458 thank Joseph Gilmore, Steve Slater, Kwan-Ki Hwang, Ahmad Yousef Abuahmad, and the Duke Human Vaccine
459 Institute Flow Cytometry Facility for flow cytometric sorting; Tyler Evangelous for purification of PCR product;
460 Caroline Jones for production of fluorophore-labeled reagents; Kara Anasti and the Duke BMI CORE facility for
461 SPR measurements of antibody affinities; Madison Berry and Sravani Venkatayogi for bioinformatics assistance;
462 Paige Rawls, Lena Smith, Jemma Hwang, Beth Bryan, Jingjing Li, Haiyan Chen for protein and DNA production
463 assistance; Nicole De Naeyer for RNA extraction assistance. We thank Drs. Matthew Gagne and Daniel C. Douek
464 at VRC/NIH for the helpful discussions regarding the subgenomic RNA assays. We thank Kelly Soderberg,
465 Elizabeth Donahue, Amelia Karlsson, Amanda Newman and Whitney Edwards for program management. COVID-
466 19 donor sample processing, flow cytometric sorting, and replication-competent virus neutralization assays were
467 performed in the Duke Regional Biocontainment Laboratory, which received partial support for construction from
468 the National Institutes of Health, National Institute of Allergy and Infectious Diseases (UC6-AI058607). This work
469 was supported by a contract from the State of NC funded by the Coronavirus Aid, Relief, and Economic Security

470 Act (CARES Act); an administrative supplement to NIH R01 AI145687 for coronavirus research (P.A.); NIH
471 grants R01AI157155 and U54CA260543 (R.S.B.); NIH NIAID U19AI142596 grant (B.F.H.); NIH R01 AI146779
472 and a Massachusetts Consortium on Pathogenesis Readiness (MassCPR) grant (A.G.S.); training grants: NIGMS
473 T32 GM007753 (B.M.H. and T.M.C); T32 AI007245 (J.F.); and a cooperative agreement with DOD/DARPA
474 (HR0011-17-2-0069; G.D.S). Cryo-EM data were collected at the National Center for Cryo-EM Access and
475 Training (NCCAT) and the Simons Electron Microscopy Center located at the New York Structural Biology
476 Center, supported by the NIH Common Fund Transformative High Resolution Cryo-Electron Microscopy program
477 (U24 GM129539,) and by grants from the Simons Foundation (SF349247) and NY State. We thank Ed Eng,
478 Carolina Hernandez and Daija Bobe for microscope alignments and assistance with cryo-EM data collection. This
479 study utilized the computational resources offered by Duke Research Computing (<http://rc.duke.edu>; NIH
480 1S10OD018164-01) at Duke University. David R. Martinez is funded by an NIH F32 AI152296, a Burroughs
481 Wellcome Fund Postdoctoral Enrichment Program Award, and was previously supported by an NIH NIAID T32
482 AI007151. We thank M. DeLong, C. Kneifel, M. Newton, V. Orlikowski, T. Milledge, and D. Lane from the Duke
483 Office of Information Technology and Research Computing for assisting with setting up and maintaining the
484 computing environment. We thank Laurent Pessaint, Anthony Cook, Alan Dodson, Katelyn Steingrebe and Bridget
485 Bart at BIOQUAL for administrative and technical assistance with non-human primate studies.

486

487 **AUTHOR CONTRIBUTIONS**

488 D.L. designed and performed experiments, analyzed data, and wrote the manuscript. R.J.E., K.Mansouri,
489 K.Manne, S.G., K.J., M.K., V.S. and P.A. performed structure experiments and analysis. R.J.E. and P.A.
490 supervised structural studies and wrote the manuscript. S.M.A. and K.C. performed and analyzed the SPR work.
491 A.S. and D.R.M. performed the mouse challenge work. D.R.M., L.V.T., T.D.S performed SARS-CoV-1 and bat
492 CoV neutralization assays. K.W. performed bioinformatic analysis of antibody sequences. X.L. performed antibody
493 isolation. R.P., V.G., and M.D. performed ELISA assay. L.L.S. oversaw the NHP study. C.T.D. and T.N.D
494 oversaw the viral RNA assay. T.H.O. and G.D.S. performed SARS-CoV-2 virus neutralization assays. E.L., A.F.,
495 F.C., G.E.H., A.S., K.T. and C.J. prepared DNA and produced antibodies. L.G.P., C.M. and D.C.M. performed
496 pseudovirus neutralization assays. M.B., T.V.H. and B.F.H. performed autoreactivity assays. C.W.W and E.P.
497 oversaw setting up the MESSI donor cohort. A.M., E.S., and R.P. performed COVID-19 donor serology. M.A.M.

498 oversaw the protein fluorescent labeling and flow cytometry sorting. D.W.C. designed and performed flow
499 cytometry sorting. A.G.S., J.F., B.M.H, T.M.C., I.T., T.Z., P.D.K., J.M. and B.G. provided key reagents for this
500 study. K.W.B., M.M., B.M.N., I.N.M., and R.S. oversaw or performed pathology experiments. H.A., and M.G.L.
501 led and performed the non-human primate studies. R.S.B. supervised the SARS-CoV-1 and bat CoV neutralization
502 assays and the mouse challenge studies. K.O.S. and B.F.H. conceived, designed and supervised the study, reviewed
503 all data, and wrote the paper. All authors reviewed and commented on the manuscript.

504

505 **DECLARATION OF INTERESTS**

506 B.F.H., G.D.S. K.O.S., R.P., D.L. and X.L. have applied for patents concerning SARS-CoV-2 antibodies that
507 are related to this work. All other authors declare no conflict of interest.

508

509 **REFERENCES**

510 Anderson, E.J., Roupheal, N.G., Widge, A.T., Jackson, L.A., Roberts, P.C., Makhene, M., Chappell, J.D.,
511 Denison, M.R., Stevens, L.J., Pruijssers, A.J., *et al.* (2020). Safety and Immunogenicity of SARS-CoV-2
512 mRNA-1273 Vaccine in Older Adults. *N Engl J Med.*
513 Arvin, A.M., Fink, K., Schmid, M.A., Cathcart, A., Spreafico, R., Havenar-Daughton, C., Lanzavecchia,
514 A., Corti, D., and Virgin, H.W. (2020). A perspective on potential antibody-dependent enhancement of
515 SARS-CoV-2. *Nature* 584, 353-363.
516 Battles, M.B., and McLellan, J.S. (2019). Respiratory syncytial virus entry and how to block it. *Nat Rev*
517 *Microbiol* 17, 233-245.
518 Baum, A., Fulton, B.O., Wloga, E., Copin, R., Pascal, K.E., Russo, V., Giordano, S., Lanza, K., Negron,
519 N., Ni, M., *et al.* (2020). Antibody cocktail to SARS-CoV-2 spike protein prevents rapid mutational
520 escape seen with individual antibodies. *Science* 369, 1014-1018.
521 Bournazos, S., Gupta, A., and Ravetch, J.V. (2020). The role of IgG Fc receptors in antibody-dependent
522 enhancement. *Nat Rev Immunol* 20, 633-643.
523 Brouwer, P.J.M., Caniels, T.G., van der Straten, K., Snitselaar, J.L., Aldon, Y., Bangaru, S., Torres, J.L.,
524 Okba, N.M.A., Claireaux, M., Kerster, G., *et al.* (2020a). Potent neutralizing antibodies from COVID-19
525 patients define multiple targets of vulnerability. *Science* 369, 643-650.
526 Brouwer, P.J.M., Caniels, T.G., van der Straten, K., Snitselaar, J.L., Aldon, Y., Bangaru, S., Torres, J.L.,
527 Okba, N.M.A., Claireaux, M., Kerster, G., *et al.* (2020b). Potent neutralizing antibodies from COVID-19
528 patients define multiple targets of vulnerability. *Science.*
529 Cao, Y., Su, B., Guo, X., Sun, W., Deng, Y., Bao, L., Zhu, Q., Zhang, X., Zheng, Y., Geng, C., *et al.*
530 (2020). Potent Neutralizing Antibodies against SARS-CoV-2 Identified by High-Throughput Single-Cell
531 Sequencing of Convalescent Patients' B Cells. *Cell* 182, 73-84 e16.
532 Chen, X., Li, R., Pan, Z., Qian, C., Yang, Y., You, R., Zhao, J., Liu, P., Gao, L., Li, Z., *et al.* (2020).
533 Human monoclonal antibodies block the binding of SARS-CoV-2 spike protein to angiotensin converting
534 enzyme 2 receptor. *Cell Mol Immunol* 17, 647-649.
535 Cheung, C.Y., Poon, L.L., Ng, I.H., Luk, W., Sia, S.F., Wu, M.H., Chan, K.H., Yuen, K.Y., Gordon, S.,
536 Guan, Y., *et al.* (2005). Cytokine responses in severe acute respiratory syndrome coronavirus-infected
537 macrophages in vitro: possible relevance to pathogenesis. *J Virol* 79, 7819-7826.

538 Chi, X., Yan, R., Zhang, J., Zhang, G., Zhang, Y., Hao, M., Zhang, Z., Fan, P., Dong, Y., Yang, Y., *et al.*
539 (2020). A potent neutralizing human antibody reveals the N-terminal domain of the Spike protein of
540 SARS-CoV-2 as a site of vulnerability.

541 Corbett, K.S., Edwards, D.K., Leist, S.R., Abiona, O.M., Boyoglu-Barnum, S., Gillespie, R.A., Himansu,
542 S., Schafer, A., Ziwawo, C.T., DiPiazza, A.T., *et al.* (2020a). SARS-CoV-2 mRNA vaccine design
543 enabled by prototype pathogen preparedness. *Nature* 586, 567-571.

544 Corbett, K.S., Flynn, B., Foulds, K.E., Francica, J.R., Boyoglu-Barnum, S., Werner, A.P., Flach, B.,
545 O'Connell, S., Bock, K.W., Minai, M., *et al.* (2020b). Evaluation of the mRNA-1273 Vaccine against
546 SARS-CoV-2 in Nonhuman Primates. *N Engl J Med* 383, 1544-1555.

547 Corti, D., and Lanzavecchia, A. (2013). Broadly neutralizing antiviral antibodies. *Annu Rev Immunol* 31,
548 705-742.

549 Dashti, A., DeVico, A.L., Lewis, G.K., and Sajadi, M.M. (2019). Broadly Neutralizing Antibodies
550 against HIV: Back to Blood. *Trends Mol Med* 25, 228-240.

551 Dekkers, G., Bentlage, A.E.H., Stegmann, T.C., Howie, H.L., Lissenberg-Thunnissen, S., Zimring, J.,
552 Rispens, T., and Vidarsson, G. (2017). Affinity of human IgG subclasses to mouse Fc gamma receptors.
553 *MAbs* 9, 767-773.

554 Dingens, A.S., Acharya, P., Haddox, H.K., Rawi, R., Xu, K., Chuang, G.Y., Wei, H., Zhang, B., Mascola,
555 J.R., Carragher, B., *et al.* (2018). Complete functional mapping of infection- and vaccine-elicited
556 antibodies against the fusion peptide of HIV. *PLoS Pathog* 14, e1007159.

557 Dinno, K.H., 3rd, Leist, S.R., Schafer, A., Edwards, C.E., Martinez, D.R., Montgomery, S.A., West, A.,
558 Yount, B.L., Jr., Hou, Y.J., Adams, L.E., *et al.* (2020a). A mouse-adapted model of SARS-CoV-2 to test
559 COVID-19 countermeasures. *Nature*.

560 Dinno, K.H., 3rd, Leist, S.R., Schafer, A., Edwards, C.E., Martinez, D.R., Montgomery, S.A., West, A.,
561 Yount, B.L., Jr., Hou, Y.J., Adams, L.E., *et al.* (2020b). A mouse-adapted model of SARS-CoV-2 to test
562 COVID-19 countermeasures. *Nature* 586, 560-566.

563 Du, L., and Jiang, S. (2010). Immunotherapy of SARS based on combinations of neutralizing human
564 monoclonal antibodies. *Future Virol* 5, 141-144.

565 FDA.gov (2020). Vaccines and Related Biological Products Advisory Committee
566 ([https://www.fda.gov/advisory-committees/advisory-committee-calendar/vaccines-and-related-biological-
567 products-advisory-committee-december-17-2020-meeting-announcement#event-materials](https://www.fda.gov/advisory-committees/advisory-committee-calendar/vaccines-and-related-biological-products-advisory-committee-december-17-2020-meeting-announcement#event-materials)).

568 Folegatti, P.M., Ewer, K.J., Aley, P.K., Angus, B., Becker, S., Belij-Rammerstorfer, S., Bellamy, D.,
569 Bibi, S., Bittaye, M., Clutterbuck, E.A., *et al.* (2020). Safety and immunogenicity of the ChAdOx1 nCoV-
570 19 vaccine against SARS-CoV-2: a preliminary report of a phase 1/2, single-blind, randomised controlled
571 trial. *Lancet* 396, 467-478.

572 Garcia-Beltran, W.F., Lam, E.C., Astudillo, M.G., Yang, D., Miller, T.E., Feldman, J., Hauser, B.M.,
573 Caradonna, T.M., Clayton, K.L., Nitido, A.D., *et al.* (2020). COVID-19 neutralizing antibodies predict
574 disease severity and survival. medRxiv.

575 Graham, B.S. (2020). Rapid COVID-19 vaccine development. *Science* 368, 945-946.

576 Group, A.-T.L.-C.S. (2020). A Neutralizing Monoclonal Antibody for Hospitalized Patients with Covid-
577 19. *New England Journal of Medicine*.

578 Gu, J., Gong, E., Zhang, B., Zheng, J., Gao, Z., Zhong, Y., Zou, W., Zhan, J., Wang, S., Xie, Z., *et al.*
579 (2005). Multiple organ infection and the pathogenesis of SARS. *J Exp Med* 202, 415-424.

580 Halstead, S.B., and Katzelnick, L. (2020). COVID-19 Vaccines: Should We Fear ADE? *J Infect Dis* 222,
581 1946-1950.

582 Hansen, J., Baum, A., Pascal, K.E., Russo, V., Giordano, S., Wloga, E., Fulton, B.O., Yan, Y., Koon, K.,
583 Patel, K., *et al.* (2020). Studies in humanized mice and convalescent humans yield a SARS-CoV-2
584 antibody cocktail. *Science* 369, 1010-1014.

585 Hassan, A.O., Case, J.B., Winkler, E.S., Thackray, L.B., Kafai, N.M., Bailey, A.L., McCune, B.T., Fox,
586 J.M., Chen, R.E., Alsoussi, W.B., *et al.* (2020). A SARS-CoV-2 Infection Model in Mice Demonstrates
587 Protection by Neutralizing Antibodies. *Cell* 182, 744-753 e744.

588 Haynes, B.F., Corey, L., Fernandes, P., Gilbert, P.B., Hotez, P.J., Rao, S., Santos, M.R., Schuitemaker,
589 H., Watson, M., and Arvin, A. (2020). Prospects for a safe COVID-19 vaccine. *Sci Transl Med* *12*.
590 Henderson, R., Edwards, R.J., Mansouri, K., Janowska, K., Stalls, V., Gobeil, S.M.C., Kopp, M., Li, D.,
591 Parks, R., Hsu, A.L., *et al.* (2020). Controlling the SARS-CoV-2 spike glycoprotein conformation. *Nat*
592 *Struct Mol Biol* *27*, 925-933.
593 Ho, M.S., Chen, W.J., Chen, H.Y., Lin, S.F., Wang, M.C., Di, J., Lu, Y.T., Liu, C.L., Chang, S.C., Chao,
594 C.L., *et al.* (2005). Neutralizing antibody response and SARS severity. *Emerg Infect Dis* *11*, 1730-1737.
595 Hou, Y.J., Okuda, K., Edwards, C.E., Martinez, D.R., Asakura, T., Dinnon, K.H., 3rd, Kato, T., Lee,
596 R.E., Yount, B.L., Mascenik, T.M., *et al.* (2020). SARS-CoV-2 Reverse Genetics Reveals a Variable
597 Infection Gradient in the Respiratory Tract. *Cell* *182*, 429-446 e414.
598 Hsieh, C.L., Goldsmith, J.A., Schaub, J.M., DiVenere, A.M., Kuo, H.C., Javanmardi, K., Le, K.C.,
599 Wrapp, D., Lee, A.G., Liu, Y., *et al.* (2020). Structure-based design of prefusion-stabilized SARS-CoV-2
600 spikes. *Science* *369*, 1501-1505.
601 Hui, K.P.Y., Cheung, M.C., Perera, R., Ng, K.C., Bui, C.H.T., Ho, J.C.W., Ng, M.M.T., Kuok, D.I.T.,
602 Shih, K.C., Tsao, S.W., *et al.* (2020). Tropism, replication competence, and innate immune responses of
603 the coronavirus SARS-CoV-2 in human respiratory tract and conjunctiva: an analysis in ex-vivo and in-
604 vitro cultures. *Lancet Respir Med* *8*, 687-695.
605 Huo, J., Le Bas, A., Ruza, R.R., Duyvesteyn, H.M.E., Mikolajek, H., Malinauskas, T., Tan, T.K., Rijal,
606 P., Dumoux, M., Ward, P.N., *et al.* (2020). Neutralizing nanobodies bind SARS-CoV-2 spike RBD and
607 block interaction with ACE2. *Nat Struct Mol Biol* *27*, 846-854.
608 Iwasaki, A., and Yang, Y. (2020). The potential danger of suboptimal antibody responses in COVID-19.
609 *Nat Rev Immunol* *20*, 339-341.
610 Jackson, L.A., Anderson, E.J., Roupael, N.G., Roberts, P.C., Makhene, M., Coler, R.N., McCullough,
611 M.P., Chappell, J.D., Denison, M.R., Stevens, L.J., *et al.* (2020). An mRNA Vaccine against SARS-CoV-
612 2 - Preliminary Report. *N Engl J Med* *383*, 1920-1931.
613 Jaume, M., Yip, M.S., Cheung, C.Y., Leung, H.L., Li, P.H., Kien, F., Dutry, I., Callendret, B., Escriou,
614 N., Altmeyer, R., *et al.* (2011). Anti-severe acute respiratory syndrome coronavirus spike antibodies
615 trigger infection of human immune cells via a pH- and cysteine protease-independent FcγRIIIb
616 pathway. *J Virol* *85*, 10582-10597.
617 Jiang, S., Hillyer, C., and Du, L. (2020). Neutralizing Antibodies against SARS-CoV-2 and Other Human
618 Coronaviruses. *Trends Immunol* *41*, 355-359.
619 Joyner, M.J., Senefeld, J.W., Klassen, S.A., Mills, J.R., Johnson, P.W., Theel, E.S., Wiggins, C.C.,
620 Bruno, K.A., Klompas, A.M., Lesser, E.R., *et al.* (2020). Effect of Convalescent Plasma on Mortality
621 among Hospitalized Patients with COVID-19: Initial Three-Month Experience. medRxiv,
622 2020.2008.2012.20169359.
623 Ju, B., Zhang, Q., Ge, J., Wang, R., Sun, J., Ge, X., Yu, J., Shan, S., Zhou, B., Song, S., *et al.* (2020).
624 Human neutralizing antibodies elicited by SARS-CoV-2 infection. *Nature* *584*, 115-119.
625 Kam, Y.W., Kien, F., Roberts, A., Cheung, Y.C., Lamirande, E.W., Vogel, L., Chu, S.L., Tse, J.,
626 Guarner, J., Zaki, S.R., *et al.* (2007). Antibodies against trimeric S glycoprotein protect hamsters against
627 SARS-CoV challenge despite their capacity to mediate FcγRIIIb-dependent entry into B cells in vitro.
628 *Vaccine* *25*, 729-740.
629 Karthik, K., Senthilkumar, T.M.A., Udhayavel, S., and Raj, G.D. (2020). Role of antibody-dependent
630 enhancement (ADE) in the virulence of SARS-CoV-2 and its mitigation strategies for the development of
631 vaccines and immunotherapies to counter COVID-19. *Hum Vaccin Immunother*, 1-6.
632 Lee, W.S., Wheatley, A.K., Kent, S.J., and DeKosky, B.J. (2020). Antibody-dependent enhancement and
633 SARS-CoV-2 vaccines and therapies. *Nat Microbiol* *5*, 1185-1191.
634 Leist, S.R., Dinnon, K.H., 3rd, Schafer, A., Tse, L.V., Okuda, K., Hou, Y.J., West, A., Edwards, C.E.,
635 Sanders, W., Fritch, E.J., *et al.* (2020a). A Mouse-Adapted SARS-CoV-2 Induces Acute Lung Injury and
636 Mortality in Standard Laboratory Mice. *Cell* *183*, 1070-1085 e1012.

637 Leist, S.R., Schafer, A., and Martinez, D.R. (2020b). Cell and animal models of SARS-CoV-2
638 pathogenesis and immunity. *Dis Model Mech* 13.

639 Liao, H.X., Levesque, M.C., Nagel, A., Dixon, A., Zhang, R., Walter, E., Parks, R., Whitesides, J.,
640 Marshall, D.J., Hwang, K.K., *et al.* (2009). High-throughput isolation of immunoglobulin genes from
641 single human B cells and expression as monoclonal antibodies. *J Virol Methods* 158, 171-179.

642 Liao, H.X., Lynch, R., Zhou, T., Gao, F., Alam, S.M., Boyd, S.D., Fire, A.Z., Roskin, K.M., Schramm,
643 C.A., Zhang, Z., *et al.* (2013). Co-evolution of a broadly neutralizing HIV-1 antibody and founder virus.
644 *Nature* 496, 469-476.

645 Liu, L., Wang, P., Nair, M.S., Yu, J., Rapp, M., Wang, Q., Luo, Y., Chan, J.F., Sahi, V., Figueroa, A., *et*
646 *al.* (2020a). Potent neutralizing antibodies against multiple epitopes on SARS-CoV-2 spike. *Nature* 584,
647 450-456.

648 Liu, Y., Soh, W.T., Tada, A., Arakawa, A., Matsuoka, S., Nakayama, E.E., Li, S., Ono, C., Torii, S.,
649 Kishida, K., *et al.* (2020b). An infectivity-enhancing site on the SARS-CoV-2 spike protein is targeted by
650 COVID-19 patient antibodies. *bioRxiv*, 2020.2012.2018.423358.

651 Menachery, V.D., Yount, B.L., Jr., Sims, A.C., Debbink, K., Agnihothram, S.S., Gralinski, L.E., Graham,
652 R.L., Scobey, T., Plante, J.A., Royal, S.R., *et al.* (2016). SARS-like WIV1-CoV poised for human
653 emergence. *Proc Natl Acad Sci U S A* 113, 3048-3053.

654 Mulligan, M.J., Lyke, K.E., Kitchin, N., Absalon, J., Gurtman, A., Lockhart, S., Neuzil, K., Raabe, V.,
655 Bailey, R., Swanson, K.A., *et al.* (2020). Phase I/II study of COVID-19 RNA vaccine BNT162b1 in
656 adults. *Nature* 586, 589-593.

657 Pak, J.E., Sharon, C., Satkunarajah, M., Auperin, T.C., Cameron, C.M., Kelvin, D.J., Seetharaman, J.,
658 Cochrane, A., Plummer, F.A., Berry, J.D., *et al.* (2009). Structural insights into immune recognition of
659 the severe acute respiratory syndrome coronavirus S protein receptor binding domain. *J Mol Biol* 388,
660 815-823.

661 Pinto, D., Park, Y.J., Beltramello, M., Walls, A.C., Tortorici, M.A., Bianchi, S., Jaconi, S., Culap, K.,
662 Zatta, F., De Marco, A., *et al.* (2020). Cross-neutralization of SARS-CoV-2 by a human monoclonal
663 SARS-CoV antibody. *Nature* 583, 290-295.

664 Polack, F.P., Thomas, S.J., Kitchin, N., Absalon, J., Gurtman, A., Lockhart, S., Perez, J.L., Perez Marc,
665 G., Moreira, E.D., Zerbini, C., *et al.* (2020). Safety and Efficacy of the BNT162b2 mRNA Covid-19
666 Vaccine. *N Engl J Med*.

667 Robbiani, D.F., Gaebler, C., Muecksch, F., Lorenzi, J.C.C., Wang, Z., Cho, A., Agudelo, M., Barnes,
668 C.O., Gazumyan, A., Finkin, S., *et al.* (2020). Convergent antibody responses to SARS-CoV-2 in
669 convalescent individuals. *Nature* 584, 437-442.

670 Rockx, B., Kuiken, T., Herfst, S., Bestebroer, T., Lamers, M.M., Oude Munnink, B.B., de Meulder, D.,
671 van Amerongen, G., van den Brand, J., Okba, N.M.A., *et al.* (2020). Comparative pathogenesis of
672 COVID-19, MERS, and SARS in a nonhuman primate model. *Science* 368, 1012-1015.

673 Rogers, T.F., Zhao, F., Huang, D., Beutler, N., Burns, A., He, W.T., Limbo, O., Smith, C., Song, G.,
674 Woehl, J., *et al.* (2020). Isolation of potent SARS-CoV-2 neutralizing antibodies and protection from
675 disease in a small animal model. *Science* 369, 956-963.

676 Schafer, A., Muecksch, F., Lorenzi, J.C.C., Leist, S.R., Cipolla, M., Bournazos, S., Schmidt, F., Maison,
677 R.M., Gazumyan, A., Martinez, D.R., *et al.* (2021). Antibody potency, effector function, and
678 combinations in protection and therapy for SARS-CoV-2 infection in vivo. *J Exp Med* 218.

679 Sempowski, G.D., Saunders, K.O., Acharya, P., Wiehe, K.J., and Haynes, B.F. (2020). Pandemic
680 Preparedness: Developing Vaccines and Therapeutic Antibodies For COVID-19. *Cell* 181, 1458-1463.

681 Shi, R., Shan, C., Duan, X., Chen, Z., Liu, P., Song, J., Song, T., Bi, X., Han, C., Wu, L., *et al.* (2020). A
682 human neutralizing antibody targets the receptor-binding site of SARS-CoV-2. *Nature* 584, 120-124.

683 Takada, A., Ebihara, H., Feldmann, H., Geisbert, T.W., and Kawaoka, Y. (2007). Epitopes required for
684 antibody-dependent enhancement of Ebola virus infection. *J Infect Dis* 196 *Suppl* 2, S347-356.

685 Ubol, S., and Halstead, S.B. (2010). How innate immune mechanisms contribute to antibody-enhanced
686 viral infections. *Clin Vaccine Immunol* 17, 1829-1835.

687 Ulrich, H., Pillat, M.M., and Tarnok, A. (2020). Dengue Fever, COVID-19 (SARS-CoV-2), and
688 Antibody-Dependent Enhancement (ADE): A Perspective. *Cytometry A* 97, 662-667.

689 Walls, A.C., Park, Y.J., Tortorici, M.A., Wall, A., McGuire, A.T., and Velesler, D. (2020). Structure,
690 Function, and Antigenicity of the SARS-CoV-2 Spike Glycoprotein. *Cell* 181, 281-292 e286.

691 Wan, Y., Shang, J., Sun, S., Tai, W., Chen, J., Geng, Q., He, L., Chen, Y., Wu, J., Shi, Z., *et al.* (2020).
692 Molecular Mechanism for Antibody-Dependent Enhancement of Coronavirus Entry. *J Virol* 94.

693 Wang, C., Li, W., Drabek, D., Okba, N.M.A., van Haperen, R., Osterhaus, A., van Kuppeveld, F.J.M.,
694 Haagsmans, B.L., Grosveld, F., and Bosch, B.J. (2020a). A human monoclonal antibody blocking SARS-
695 CoV-2 infection. *Nat Commun* 11, 2251.

696 Wang, Q., Zhang, L., Kuwahara, K., Li, L., Liu, Z., Li, T., Zhu, H., Liu, J., Xu, Y., Xie, J., *et al.* (2016).
697 Immunodominant SARS Coronavirus Epitopes in Humans Elicited both Enhancing and Neutralizing
698 Effects on Infection in Non-human Primates. *ACS Infect Dis* 2, 361-376.

699 Wang, Q., Zhang, Y., Wu, L., Niu, S., Song, C., Zhang, Z., Lu, G., Qiao, C., Hu, Y., Yuen, K.Y., *et al.*
700 (2020b). Structural and Functional Basis of SARS-CoV-2 Entry by Using Human ACE2. *Cell* 181, 894-
701 904 e899.

702 Wang, S.F., Tseng, S.P., Yen, C.H., Yang, J.Y., Tsao, C.H., Shen, C.W., Chen, K.H., Liu, F.T., Liu,
703 W.T., Chen, Y.M., *et al.* (2014). Antibody-dependent SARS coronavirus infection is mediated by
704 antibodies against spike proteins. *Biochem Biophys Res Commun* 451, 208-214.

705 Wec, A.Z., Wrapp, D., Herbert, A.S., Maurer, D.P., Haslwanter, D., Sakharkar, M., Jangra, R.K.,
706 Dieterle, M.E., Lilov, A., Huang, D., *et al.* (2020). Broad neutralization of SARS-related viruses by
707 human monoclonal antibodies. *Science* 369, 731-736.

708 Wrapp, D., De Vlioger, D., Corbett, K.S., Torres, G.M., Wang, N., Van Breedam, W., Roose, K., van
709 Schie, L., Team, V.-C.C.-R., Hoffmann, M., *et al.* (2020a). Structural Basis for Potent Neutralization of
710 Betacoronaviruses by Single-Domain Camelid Antibodies. *Cell* 181, 1004-1015 e1015.

711 Wrapp, D., Wang, N., Corbett, K.S., Goldsmith, J.A., Hsieh, C.L., Abiona, O., Graham, B.S., and
712 McLellan, J.S. (2020b). Cryo-EM structure of the 2019-nCoV spike in the prefusion conformation.
713 *Science* 367, 1260-1263.

714 Wu, F., Yan, R., Liu, M., Liu, Z., Wang, Y., Luan, D., Wu, K., Song, Z., Sun, T., Ma, Y., *et al.* (2020a).
715 Antibody-dependent enhancement (ADE) of SARS-CoV-2 infection in recovered COVID-19 patients:
716 studies based on cellular and structural biology analysis. medRxiv, 2020.2010.2008.20209114.

717 Wu, Y., Wang, F., Shen, C., Peng, W., Li, D., Zhao, C., Li, Z., Li, S., Bi, Y., Yang, Y., *et al.* (2020b). A
718 noncompeting pair of human neutralizing antibodies block COVID-19 virus binding to its receptor
719 ACE2. *Science* 368, 1274-1278.

720 Xu, J., Jia, W., Wang, P., Zhang, S., Shi, X., Wang, X., and Zhang, L. (2019). Antibodies and vaccines
721 against Middle East respiratory syndrome coronavirus. *Emerg Microbes Infect* 8, 841-856.

722 Xu, K., Acharya, P., Kong, R., Cheng, C., Chuang, G.Y., Liu, K., Louder, M.K., O'Dell, S., Rawi, R.,
723 Sastry, M., *et al.* (2018). Epitope-based vaccine design yields fusion peptide-directed antibodies that
724 neutralize diverse strains of HIV-1. *Nat Med* 24, 857-867.

725 Yilla, M., Harcourt, B.H., Hickman, C.J., McGrew, M., Tamin, A., Goldsmith, C.S., Bellini, W.J., and
726 Anderson, L.J. (2005). SARS-coronavirus replication in human peripheral monocytes/macrophages.
727 *Virus Res* 107, 93-101.

728 Yip, M.S., Leung, H.L., Li, P.H., Cheung, C.Y., Dutry, I., Li, D., Daeron, M., Bruzzone, R., Peiris, J.S.,
729 and Jaume, M. (2016). Antibody-dependent enhancement of SARS coronavirus infection and its role in
730 the pathogenesis of SARS. *Hong Kong Med J* 22, 25-31.

731 Yip, M.S., Leung, N.H., Cheung, C.Y., Li, P.H., Lee, H.H., Daeron, M., Peiris, J.S., Bruzzone, R., and
732 Jaume, M. (2014). Antibody-dependent infection of human macrophages by severe acute respiratory
733 syndrome coronavirus. *Virol J* 11, 82.

734 Zhou, D., Duyvesteyn, H.M.E., Chen, C.P., Huang, C.G., Chen, T.H., Shih, S.R., Lin, Y.C., Cheng, C.Y.,
735 Cheng, S.H., Huang, Y.C., *et al.* (2020). Structural basis for the neutralization of SARS-CoV-2 by an
736 antibody from a convalescent patient. *Nat Struct Mol Biol* 27, 950-958.

737 Zhou, J., Chu, H., Li, C., Wong, B.H., Cheng, Z.S., Poon, V.K., Sun, T., Lau, C.C., Wong, K.K., Chan,
738 J.Y., *et al.* (2014). Active replication of Middle East respiratory syndrome coronavirus and aberrant
739 induction of inflammatory cytokines and chemokines in human macrophages: implications for
740 pathogenesis. *J Infect Dis* 209, 1331-1342.

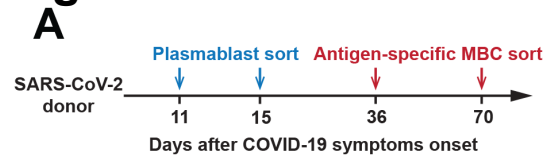
741 Zost, S.J., Gilchuk, P., Case, J.B., Binshtein, E., Chen, R.E., Nkolola, J.P., Schafer, A., Reidy, J.X.,
742 Trivette, A., Nargi, R.S., *et al.* (2020a). Potently neutralizing and protective human antibodies against
743 SARS-CoV-2. *Nature* 584, 443-449.

744 Zost, S.J., Gilchuk, P., Chen, R.E., Case, J.B., Reidy, J.X., Trivette, A., Nargi, R.S., Sutton, R.E.,
745 Suryadevara, N., Chen, E.C., *et al.* (2020b). Rapid isolation and profiling of a diverse panel of human
746 monoclonal antibodies targeting the SARS-CoV-2 spike protein. *Nat Med* 26, 1422-1427.

747

748

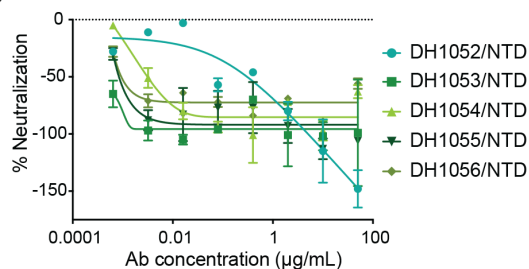
Figure 1



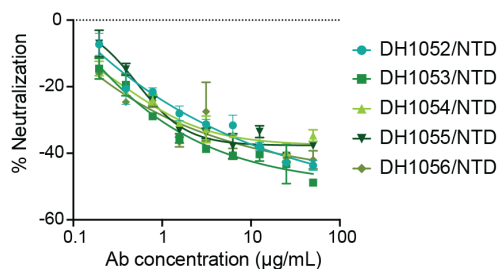
C

Donor	Cell Type	B cells sorted	SARS-CoV-2 Abs	RBD	NTD	S2	Spike only	NP
SARS-CoV-2 donor	Plasmablasts	773	101	11	4	42	1	43
SARS-CoV-2 donor	Memory B cells	594	307	121	58	99	29	NA
SARS-CoV-1 donor	Memory B cells	370	55	18	7	7	23	NA
Total		1737	463	150	69	148	53	43
Down-selected for production		NA	187	81	41	65	0	0

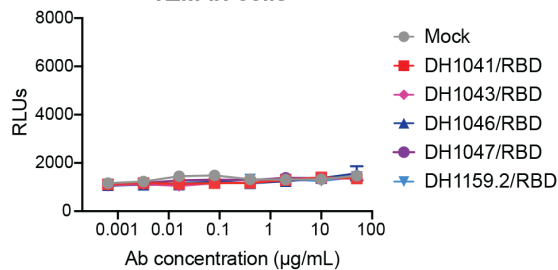
D Pseudovirus in 293T/ACE2 cells



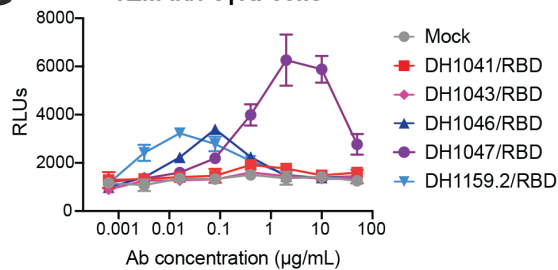
E SARS-CoV-2 in Vero cells



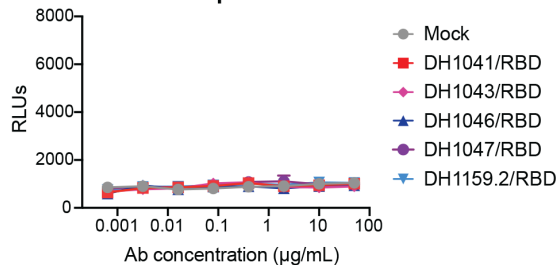
F TZM-bl cells



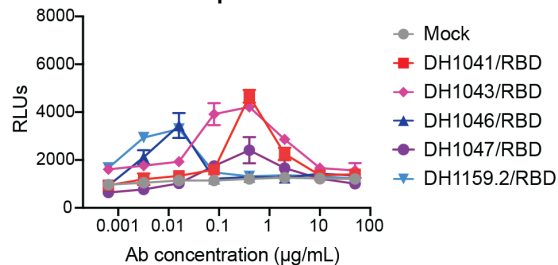
G TZM-bl/FcγRI cells



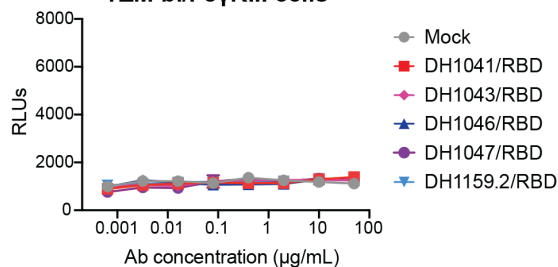
H TZM-bl/FcγRIIIa cells



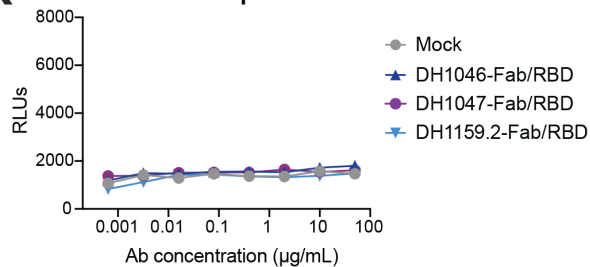
I TZM-bl/FcγRIIIb cells



J TZM-bl/FcγRIIIc cells



K TZM-bl/FcγRI cells



L TZM-bl/FcγRIIIb cells

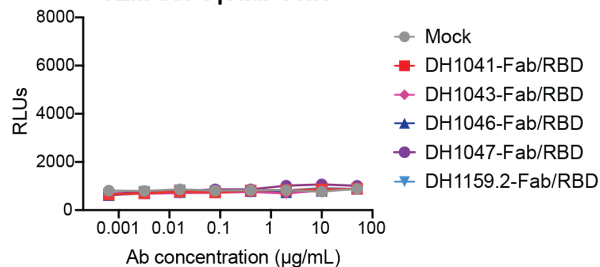


Figure 1. SARS-CoV-2 receptor-binding domain (RBD) and N-terminal domain (NTD) antibodies mediate FcγR-dependent and FcγR-independent enhancement of SARS-CoV-2 infection respectively.

(A-B) Timeline of blood sampling and antibody isolation from convalescent SARS-CoV-2 and SARS-CoV-1 donors. Plasmablasts and/or antigen-specific memory B cells (MBC) were sorted from a (A) SARS-CoV-2 infected individual (SARS-CoV-2 donor) and a (B) 2003 SARS survivor (SARS-CoV-1 donor).

(C) Summary of number and specificity of antibodies isolated from each donor.

(D-E) FcγR-independent SARS-CoV-2 infection-enhancement mediated by non-neutralizing NTD antibodies. *In vitro* neutralization curves for NTD infection-enhancing antibodies against (D) pseudotyped SARS-CoV-2 D614G in 293T-hACE2 cells, and (E) replication-competent nano-luciferase (nLuc) SARS-CoV-2 in Vero cells.

(F-J) FcγR-dependent SARS-CoV-2 infection-enhancement in ACE2-negative cells mediated by neutralizing RBD antibodies. Pseudotyped SARS-CoV-2 incubated with RBD antibodies or mock medium control were inoculated on (F) parental TZM-bl cells, and TZM-bl cells stably expressing human FcγR receptors (G) FcγRI, (H) FcγRIIa, (I) FcγRIIb or (J) FcγRIII.

(K-L) The effect of RBD antibody fragment antigen-binding regions (Fabs) on pseudotyped SARS-CoV-2 D614G infection were tested in (K) FcγRI-expressing TZM-bl cells and (L) FcγRIIb-expressing TZM-bl cells. Relative luminescence units (RLUs) were measured in cell lysate at 68-72 hours post-infection. Upward deflection of RLUs in the presence of antibody indicates FcγR-mediated infection. Three or four independent experiments were performed and representative data are shown.

Figure 2

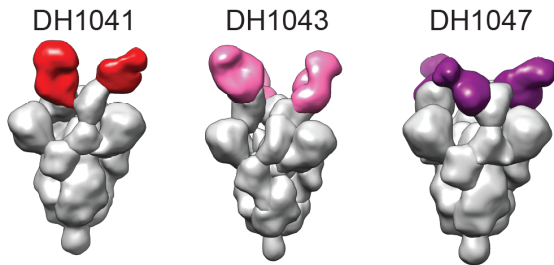
A

Antibody	Epitope	Effect on SARS-CoV-2 infection		Cross-reactivity with SARS-CoV-1	ACE2 blocking		SARS-CoV-2 pseudovirus			SARS-CoV-2 replication competent virus			Effect on SARS-CoV-2 infection
		ACE2 ^{pos} FcγR ^{neg} cells	ACE2 ^{neg} FcγR ^{pos} cells		IC ₅₀	IC ₈₀	IC ₅₀	IC ₈₀	Maximal% inhibition	MN titer	IC ₅₀	IC ₈₀	
DH1041	RBD				0.036	0.497	0.017	0.049	>100	0.098	0.016	0.063	Neutralizing
DH1043	RBD				0.043	0.280	0.0015	0.020	>100	0.098	0.034	0.099	
DH1159.2	RBD				>50	>50	11,900	>50	77.0	>100	ND	ND	Infection-enhancing
DH1046	RBD				0.201	6.512	0.396	2.030	>100	12.500	1.086	9.383	
DH1047	RBD				0.078	0.567	0.090	0.360	>100	1.100	0.124	0.666	Non-reactive
DH1042	RBD				0.059	0.371	0.011	0.053	>100	0.280	0.071	0.269	
DH1044	RBD				>50	>50	0.021	0.080	98.0	0.550	0.076	0.273	Neutralizing
DH1045	RBD				0.226	24.353	0.380	2.260	>100	6.250	1.437	4.827	
DH1052	NTD				>50	>50	>50	>50	-148.0	>100	>100	>100	Infection-enhancing
DH1053	NTD				>50	>50	>50	>50	-99.0	>100	>100	>100	
DH1054	NTD				>50	>50	>50	>50	-63.0	>100	>100	>100	Infection-enhancing
DH1055	NTD				>50	>50	>50	>50	-106.0	>100	>100	>100	
DH1056	NTD				>50	>50	>50	>50	-56.0	>100	>100	>100	Infection-enhancing
DH1048	NTD				>50	>50	0.520	>50	72.0	0.390	0.608	2.232	
DH1049	NTD				>50	>50	>50	>50	49.0	0.390	0.385	3.539	Infection-enhancing
DH1050.2	NTD				>50	>50	0.280	>50	67.0	0.780	0.087	1.187	
DH1051	NTD				>50	>50	0.049	>50	68.0	0.780	0.134	0.737	Infection-enhancing
DH1050.1	NTD				>50	>50	0.039	>50	62.0	0.780	0.161	0.614	

B

Infection-enhancing RBD Ab

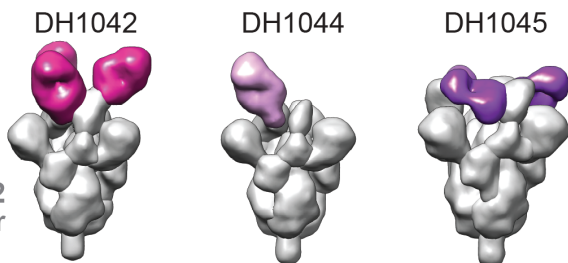
SARS-CoV-2 S trimer



C

Non-infection-enhancing RBD Ab

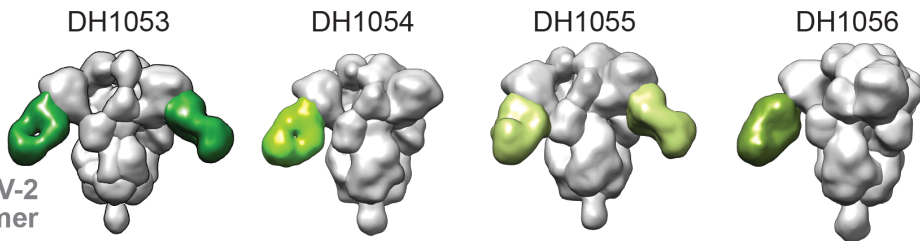
SARS-CoV-2 S trimer



D

Infection-enhancing NTD Ab

SARS-CoV-2 S trimer



E

Non-infection-enhancing NTD Ab

SARS-CoV-2 S trimer

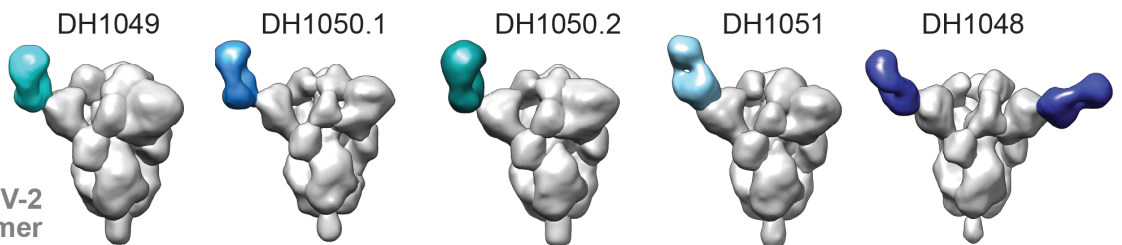


Figure 2. Structural and phenotypic characterization of infection-enhancing and non-infection-enhancing RBD and NTD antibodies.

(A) Phenotypic summary of antibodies selected for in-depth characterization. Antibody functions are color-coded based on the key shown at the right. The heatmap denotes for each antibody the epitope location, neutralizing or infection-enhancing activity in ACE2-positive/FcγR-negative cells or ACE2-negative/FcγR-positive cells. Additionally, the heatmap indicates the ability of each antibody to bind to SARS-CoV-1 S protein by ELISA, the ability of each antibody to block ACE2 binding to SARS-CoV-2 S protein, and neutralization titers against SARS-CoV-2 pseudovirus and replication-competent virus. MN titer, micro-neutralization titer; ND, not determined.

(B-E) 3D reconstruction of negative stain electron microscopy images of SARS-CoV-2 Spike ectodomain trimers stabilized with 2 proline mutations (S-2P; gray) bound to (B) infection-enhancing RBD antibody Fabs, (C) non-infection-enhancing RBD antibody Fabs, (D) infection-enhancing NTD antibody Fabs, (E) non-infection-enhancing NTD antibody Fabs. Fabs are pseudo-colored according to the phenotypic category to which they belong.

Figure 3

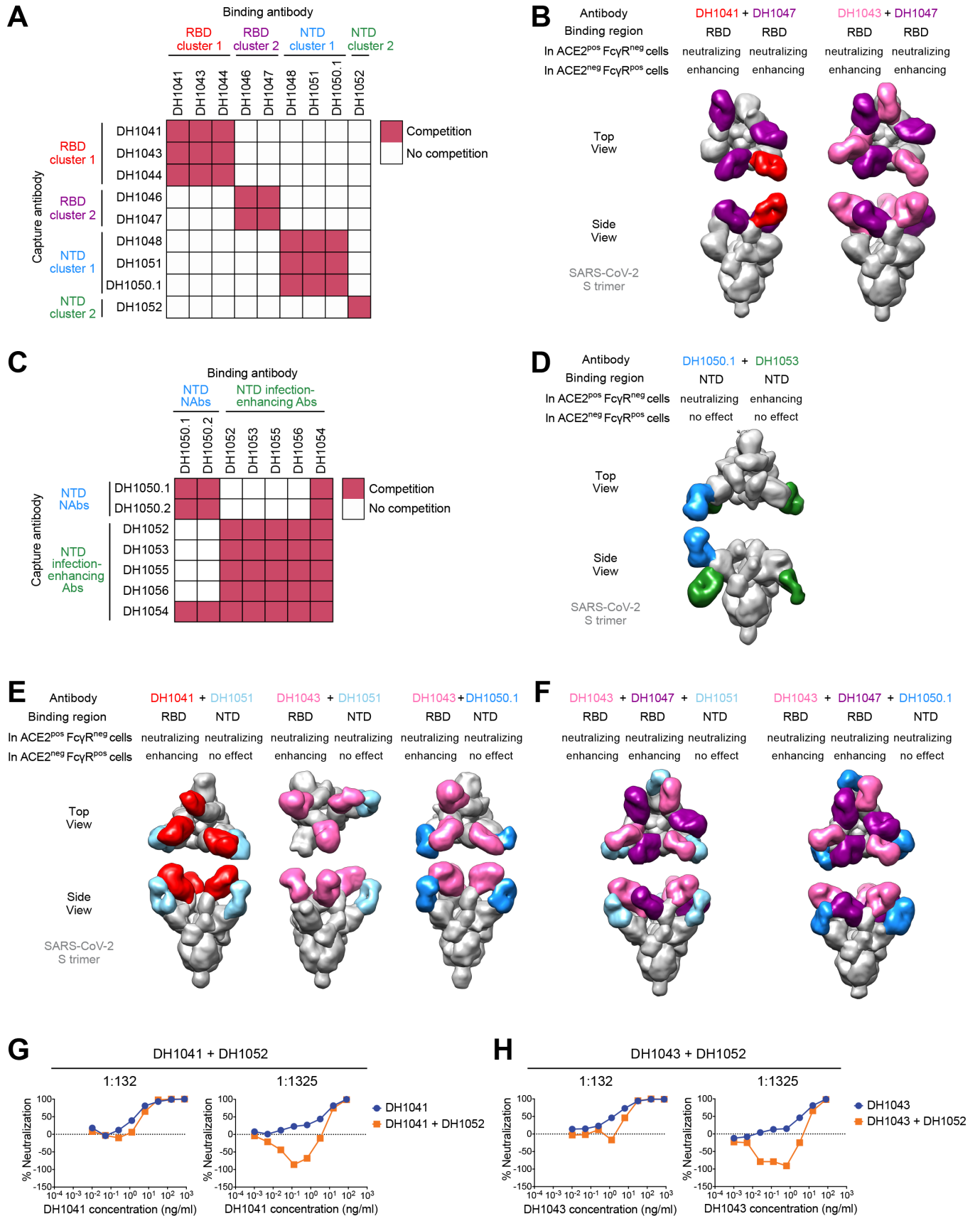


Figure 3. Biophysical and structural determination that infection-enhancing and non-infection enhancing antibodies can simultaneously bind to the same S protein.

(A) Cross-blocking activity of RBD and NTD neutralizing antibodies tested by surface plasmon resonance (SPR). Soluble, stabilized SARS-CoV-2 S trimer (S-2P) was captured by the antibody on the Y-axis followed by binding by the antibody on the X-axis. Antibody binding was considered competitive (red squares) if the binding antibody did not react with the captured S protein.

(B) 3D reconstruction of simultaneous recognition of SARS-CoV-2 S-2P trimer by two RBD antibodies DH1041+DH1047, or DH1043+DH1047. All three antibodies are SARS-CoV-2 infection-enhancing in ACE2-negative/FcγR-positive cells, but neutralizing in ACE2-positive/FcγR-negative cells.

(C) Cross-blocking activity of neutralizing antibodies and infection-enhancing NTD antibodies tested by SPR. SARS-CoV-2 S-2P trimer was captured by the antibody on the Y-axis followed by binding by the antibody on the X-axis. Antibody binding was considered competitive (red squares) if the binding antibody did not react with the captured S protein.

(D) 3D reconstruction of by NTD antibodies DH1053 and DH1050.1 simultaneously bound to SARS-CoV-2 S trimer protein. In ACE2-positive/FcγR-negative cells, DH1050.1 is neutralizing while DH1053 enhances SARS-CoV-2 infection. Both antibodies have no effect in ACE2-negative/FcγR-positive cells.

(E) 3D reconstruction of SARS-CoV-2 S protein simultaneously bound to a RBD infection-enhancing antibody and a NTD non-infection-enhancing antibody. All of these antibodies neutralize SARS-CoV-2 infection of ACE2-positive/FcγR-negative cells.

(F) 3D reconstruction of SARS-CoV-2 S protein bound to triple-antibody combinations of RBD antibody DH1043, RBD antibody DH1047, and either NTD antibody DH1051 (left) or DH1050.1 (right). Both RBD antibodies enhance SARS-CoV-2 infection of ACE2-negative/FcγR-positive cells, but neutralize infection of ACE2-positive/FcγR-negative cells. NTD antibodies DH1051 and DH1050.1 neutralize SARS-CoV-2 infection of ACE2-negative/FcγR-positive cells, but have no effect on infection of ACE2-negative/FcγR-positive cells.

(G-H) RBD antibody neutralization of SARS-CoV-2 pseudovirus infection of ACE2-expressing cells in the presence of infection-enhancing NTD antibody DH1052. The infection-enhancing NTD antibody DH1052 was mixed with RBD antibodies DH1041 **(G)** or DH1043 **(H)** in 1:132 ratio or 1:1,325 ratio, respectively. Serial dilutions of the NTD:RBD antibody mixtures (orange), as well as RBD antibody alone (blue) were examined for neutralization of SARS-CoV-2 D614G pseudovirus infection of 293T/ACE2 cells.

Figure 4

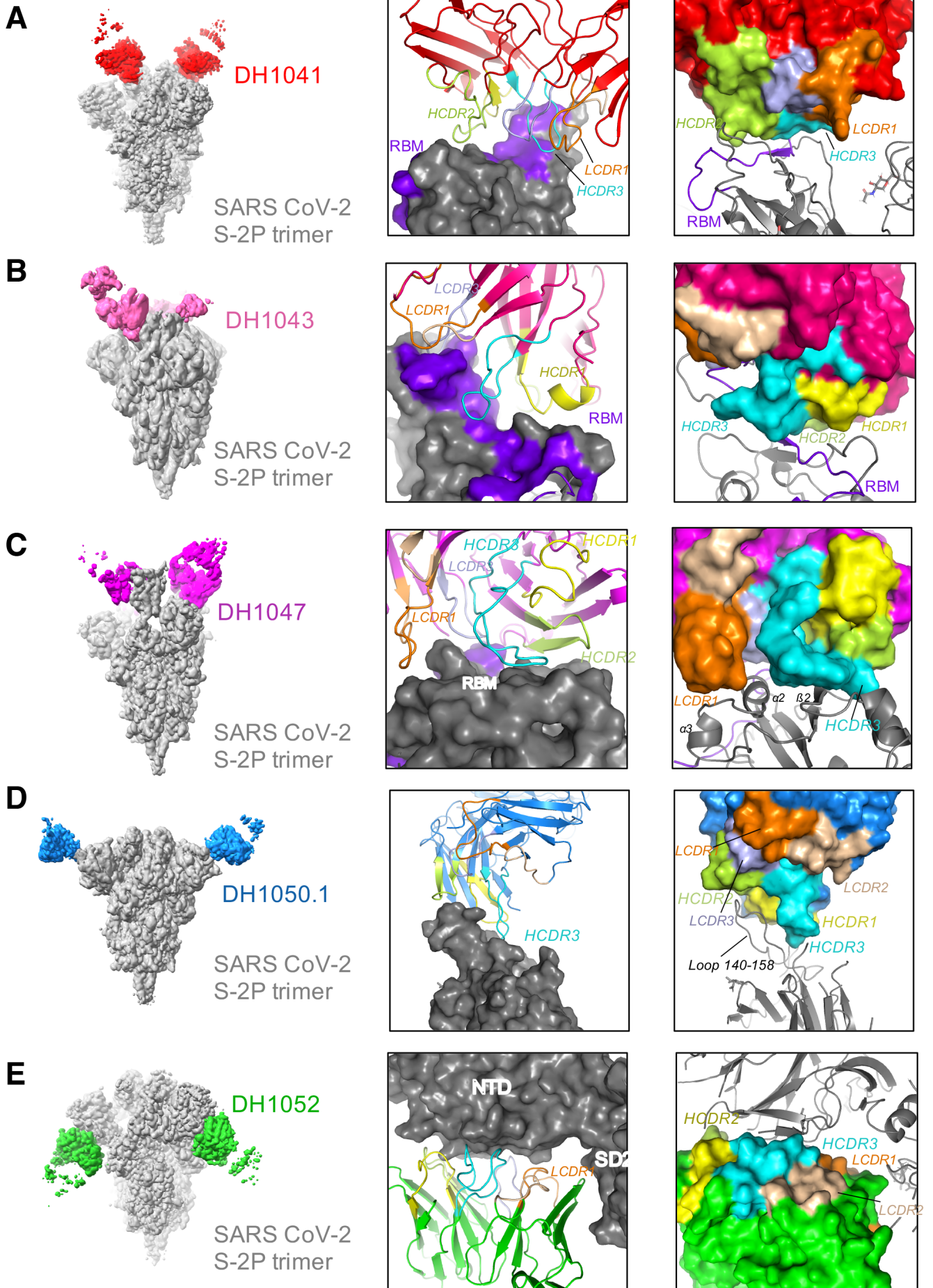


Figure 4. Cryo-electron microscopy of neutralizing and non-neutralizing antibodies in complex with SARS-CoV-2 Spike ectodomain. Structures of SARS-CoV-2 S protein in complex with RBD antibodies (A) DH1041 (red), (B) DH1043 (pink), (C) DH1047 (magenta), (D) neutralizing NTD antibody DH1050.1 (blue), and (E) infection-enhancing NTD antibody DH1052 (green). Each antibody is bound to Spike ectodomain stabilized with 2 proline mutations (S-2P) shown in gray with its Receptor Binding Motif (RBM) colored purple blue. (Right) Zoomed-in views of the antibody interactions with S-2P trimers. The antibody complementarity determining (CDR) loops are colored: HCDR1 yellow, HCDR2 limon, HCDR3 cyan, LCDR1 orange, LCDR2 wheat and LCDR3 light blue.

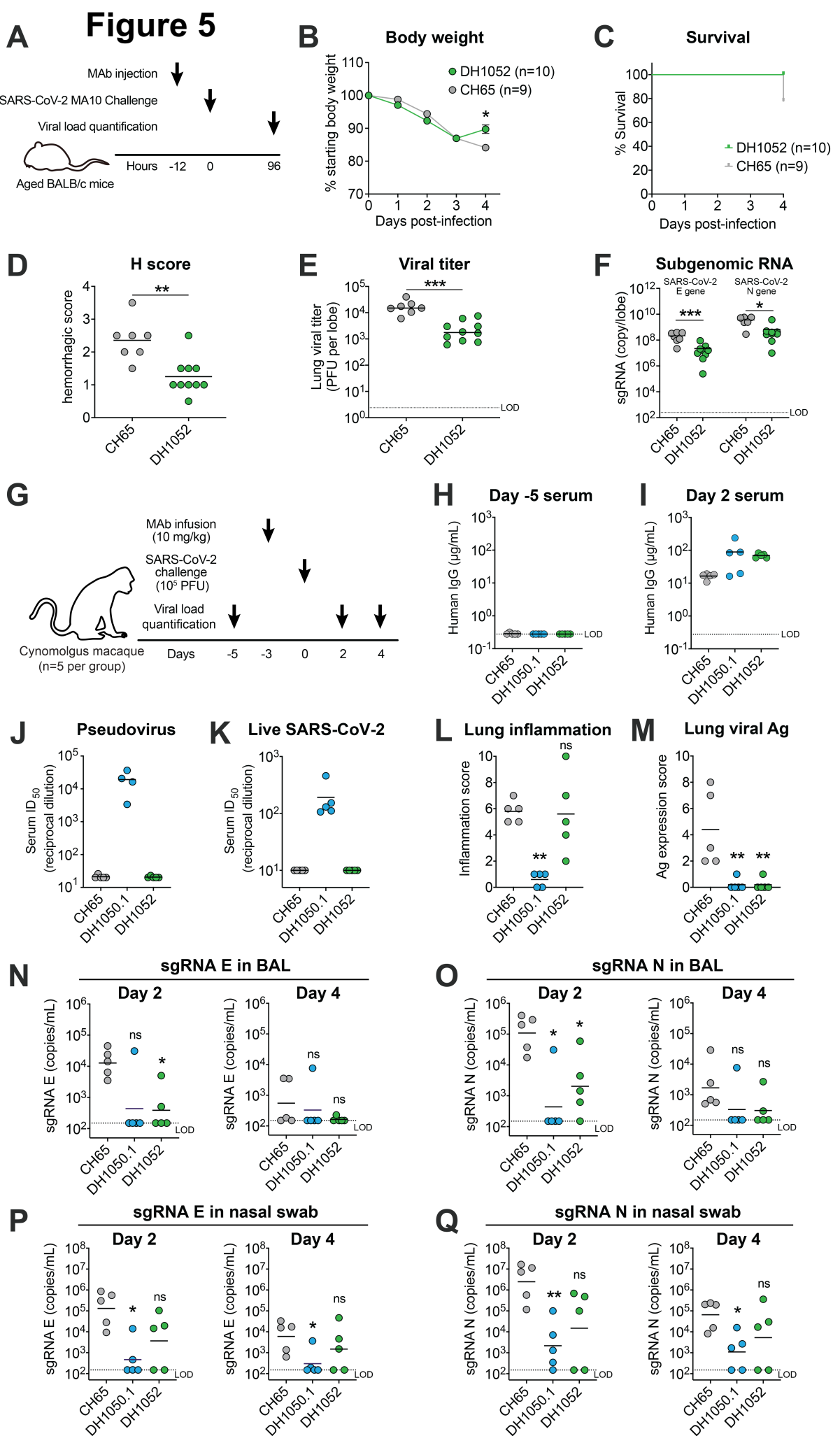


Figure 5. NTD antibody DH1052 enhances SARS-CoV-2 infection *in vitro*, but does not always enhance SARS-CoV-2 replication or disease *in vivo*.

(A-F) DH1052 passive immunization and murine SARS-CoV-2 challenge study design and outcome. **(A)** Diagram of the study design showing 52 week old female BALB/c mice were i.p. injected with DH1052 (200 µg/mouse, n=10, green symbols) or CH65 control antibody (gray, 200 µg/mouse, n=9, gray symbols). After 12 hours, mice were challenged with 1×10^4 PFU of mouse-adapted SARS-CoV-2 MA10 virus. Mice were euthanized and tissues were harvested 96 hours post-infection. **(B)** Body weight and **(C)** survival were monitored daily. **(D)** Hemorrhagic scores, **(E)** lung viral titers, as well as **(F)** viral subgenomic RNA (sgRNA) for both SARS-CoV-2 envelope (E) and nucleocapsid (N) gene were measured 96 hours post-infection.

(G-Q) Reduction of SARS-CoV-2 replication and disease in cynomolgus macaques by prophylactic administration of an NTD neutralizing antibody DH1050.1 or an *in vitro* infection-enhancing NTD Ab DH1052.

(G) Diagram of the macaque study design showing cynomolgus macaques (n=5 per group) were infused with DH1052, DH1050.1 or an irrelevant control CH65 antibody 3 days before 10^5 PFU of SARS-CoV-2 challenge via intranasal and intratracheal routes. Viral load including viral RNA and subgenomic RNA (sgRNA) were measured at the indicated pre-challenge and post-challenge timepoints. Lungs were harvested on Day 4 post-challenge for histopathology analysis.

(H-I) Serum human IgG concentrations at **(H)** Day -5 and **(I)** Day 2.

(J-K) Day 2 serum neutralization titers shown as the reciprocal serum dilution that inhibits 50% (ID₅₀) of **(J)** pseudotyped SARS-CoV-2 replication in 293T/ACE2 cells or **(K)** SARS-CoV-2 replication in Vero cells.

(L-M) Lung histopathology. Sections of the left caudal (Lc), right middle (Rm), and right caudal (Rc) lung were evaluated and scored for the presence of **(L)** inflammation by hematoxylin and eosin (H&E) staining, and for the presence of **(M)** SARS-CoV-2 nucleocapsid by immunohistochemistry (IHC) staining. Symbols indicate the sums of Lc, Rm, and Rc scores in each animal.

(N-O) SARS-CoV-2 **(N)** E gene sgRNA and **(O)** N gene sgRNA in bronchoalveolar lavage (BAL) on Day 2 and Day 4 post challenge.

(P-Q) SARS-CoV-2 **(P)** E gene sgRNA and **(Q)** N gene sgRNA in nasal swab on Day 2 and Day 4 post challenge.

LOD, limit of detection. Statistical significance in all the panels were determined using Wilcoxon rank sum exact test. Asterisks show the statistical significance between indicated group and CH65 control group: ns, not significant, *P<0.05, **P<0.001, ***P<0.0001.

Figure 6

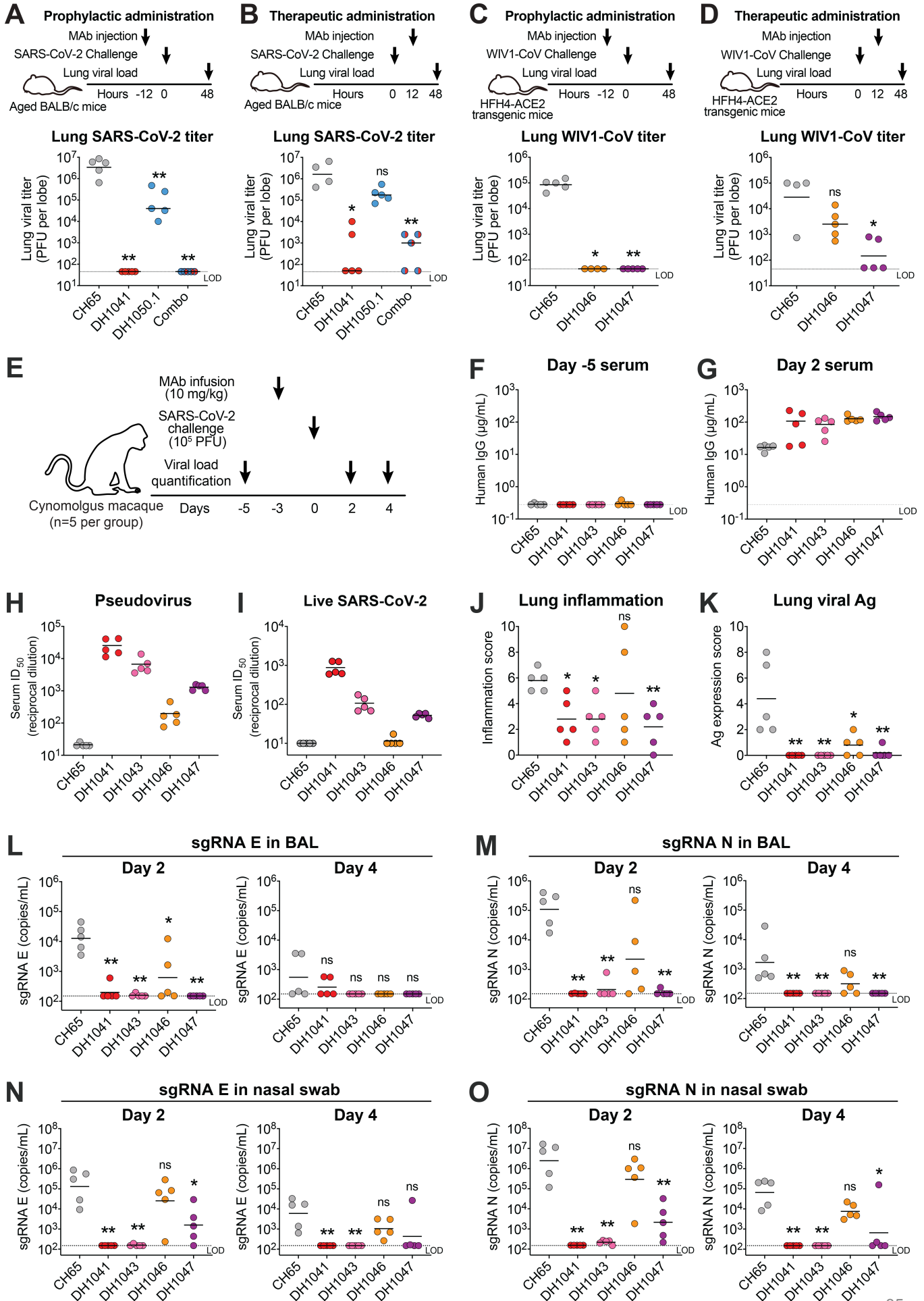


Figure 6. RBD antibodies that mediate FcγR-dependent infection enhancement *in vitro*, protect mice and non-human primates from SARS-CoV-2 challenge.

(A-B) Protection in BALB/c mice against mouse-adapted SARS-CoV-2. Mice (n=5 per group) were intraperitoneally (i.p.) injected with 300 µg of a single antibody or 150 µg of two antibodies in combination (A) prophylactically at 12h pre-infection or (B) therapeutically at 12h post-infection. Infection was performed with mouse-adapted SARS-CoV-2 2AA MA virus via intranasal (i.n.) route. Titers of infectious virus in the lung were examined 48 post-infection. An irrelevant human antibody CH65 was used as a negative control.

(C-D) Protection in HFH4-hACE2-transgenic mice against SARS-related bat WIV1-CoV challenge. Mice (n=5 per group) were intraperitoneally (i.p.) injected with 300 µg of indicated antibody or CH65 control antibody (C) prophylactically at 12h pre-infection or (D) therapeutically at 12h post-infection. Infection was performed with WIV1-CoV via i.n. route. Lung viral titers were examined at 48 post-infection.

(E-O) RBD NAbs and infection-enhancing Abs protected SARS-CoV-2 infection in non-human primates.

(E) Study design. Cynomolgus macaques (n=5 per group) were infused with DH1041, DH1043, DH1046, DH1047 or an irrelevant CH65 antibody 3 days before 10⁵ PFU of SARS-CoV-2 challenge via intranasal route and intratracheal route. Viral load including viral RNA and subgenomic RNA (sgRNA) were measured on the indicated pre-challenge and post-challenge timepoints. Lungs were harvested on Day 4 post-challenge for histopathology study.

(F-G) Serum human IgG concentrations at Day -5 (H) and Day 2 (I).

(H-I) Day 2 serum neutralization titers shown as the reciprocal serum dilution that inhibits 50% (ID₅₀) of (H) pseudotyped SARS-CoV-2 replication in 293T/ACE2 cells or (J) SARS-CoV-2 replication in Vero cells.

(J-K) Lung histopathology. Sections of the left caudal (Lc), right middle (Rm), and right caudal (Rc) lung were evaluated and scored for (J) the presence of inflammation by hematoxylin and eosin (H&E) staining, and (K) for the presence of SARS-CoV-2 nucleocapsid by immunohistochemistry (IHC) staining. Symbols indicate the sums of Lc, Rm, and Rc scores for each animal.

(L-M) SARS-CoV-2 (L) E gene sgRNA and (M) N gene sgRNA in bronchoalveolar lavage (BAL) on Day 2 and Day 4 post challenge.

(N-O) SARS-CoV-2 (N) E gene sgRNA and (O) N gene sgRNA in nasal swab on Day 2 and Day 4 post challenge.

Statistical significance in all the panels were determined using Wilcoxon rank sum exact test. Asterisks show the statistical significance between indicated group and CH65 control group: ns, not significant, *P<0.05, **P<0.001.